Semiannual Status Report No. 9 on

PROPAGATION AND DISPERSION OF HYDROMAGNETIC AND ION CYCLOTRON WAVES IN PLASMAS IMMERSED IN MAGNETIC FIELDS

July 15, 1967

Period Covered: January 15, 1967 through July 14, 1967

Research Grant NsG-353
Office of Grants and Research Contracts
Code SC
National Aeronautics and Space Administration
Washington, D.C. 20546

PLASMA DYNAMICS RESEARCH LABORATORY
DEPARTMENT OF ELECTRICAL ENGINEERING
THE UNIVERSITY OF TEXAS
AUSTIN, TEXAS 78712

Semiannual Status Report No. 9 on

PROPAGATION AND DISPERSION OF HYDROMAGNETIC AND ION CYCLOTRON WAVES IN PLASMAS IMMERSED IN MAGNETIC FIELDS

July 15, 1967

Period Covered: January 15, 1967 through July 14, 1967

Electrophysics Research Division
Attn: Dr. Harry Harrison, Chief and Dr. Karlheinz Thom
Research Grant NsG-353
Office of Grants and Research Contracts, Code SC
National Aeronautics and Space Administration
Washington, D.C. 20546

PLASMA DYNAMICS RESEARCH LABORATORY
DEPARTMENT OF ELECTRICAL ENGINEERING
THE UNIVERSITY OF TEXAS
AUSTIN, TEXAS 78712

Faculty Member Initiator and Principal Investigator:
Dr. Arwin A. Dougal
Professor of Electrical Engineering

TABLE OF CONTENTS

ABSTRACT

Theoretical investigations concerned with efficiency of rf power transfer to a cylindrical plasma are presented. The relationships between the six magnetic and electric wave field components are derived for the quasistatic case. Through suitable approximations, relations between the various wave field components are developed so that each of the components may be expressed in terms of quantities measurable in the laboratory. A method is proposed for determining wave power flow from magnetic probe measurements.

Experimental measurements of rf power coupling to the plasma are described. A measurement of phase shift is described, with initial results indicating very large $\lambda_{\parallel}$. Results from the wavelength measurement are compared to theoretical calculations of $\lambda_{\parallel}$ based on measured electron densities. Observations of complex fine structure in the wave magnetic signal are also reported.

Evidence of non-resonant coupling of rf power to the plasma is discussed. The so-called "Mode X" which is thought to be responsible is described, along with suggestions for its elimination, involving improved Faraday shielding of the Stix Coil.

An investigation of waves which propagate at low magnetic fields ($B_o \lesssim 1000$ G) is reported. These waves, which have been previously referred to as the so-called "fast" or compressional hydromagnetic waves, are found to propagate in "bands", or ranges of magnetic field. These "propagation bands" are separated by "stop bands", or ranges of magnetic field for which the waves appear attenuated.

It is found that during the strongest wave propagation, in the central "propagation band", electron density increases by more than a factor of two. Plasma diamagnetism is found to decrease, however, indicating a net loss of energy per ion. An optimum pressure is found, at which wave amplitude and electron density are at a maximum.

The study of nonlinear frequency phenomena is continued and extended to low magnetic field waves. Distortion of magnetic signal is found to increase strongly during wave attenuation. A comparison of the frequency spectra of wave magnetic signal ($\dot{b}_z$) and Stix Coil current during the rf heating cycle verify that the harmonic frequency generation occurs in the plasma rather than in the rf transmitter.

FACULTY AND STAFF

The following individuals contributed to one or more areas of the research in progress at various times during the period January 15, 1967 to July 14, 1967.

1. Dr. Arwin A. Dougal; Professor of Electrical Engineering, and Principal Investigator.

2. Jimmy G. Melton; Doctoral Candidate, and Research Engineer Assistant III.

3. Nathan B. Dodge; Doctoral Candidate, and Research Engineer Assistant III.

4. Glenn C. Andrew; Undergraduate and Laboratory Research Assistant I.

5. Miss Nancy Bagley; Senior Secretary.

PAPERS PRESENTED, LECTURES, AND PUBLICATIONS BY FACULTY AND STAFF*

A. Papers Presented:

1. Marion O. Hagler and Arwin A. Dougal, "Resonant Faraday Rotation in a Magnetoplasma-Filled Optical Resonator," 1967 Southwestern Meeting of the American Physical Society, Austin, Texas, February 23-25, 1967.

2. Frederic Weigl, Otto M. Friedrich, Jr. and Arwin A. Dougal, "Laser-Illuminated Mach-Zehnder Interferometry of a Laser-Induced Plasma," 1967 Southwestern Meeting of the American Physical Society, Austin, Texas, February 23-25, 1967.

3. Arwin A. Dougal, "Holography, Laser, and Plasma Studies," Proceedings of the Fourth Annual Joint Services Electronics Program Review, The University of Texas, Austin, Texas, March 16-17, 1967.

4. Frederic Weigl, Otto M. Friedrich, Jr. and Arwin A. Dougal, "Mach-Zehnder Interferometry of Laser-Induced Plasmas in Atmospheric and Super-High Pressure Gases," Texas Academy of Science Annual Meeting, Texas A&M University, College Station, Texas, April 19-21, 1967.

5. Frederic Weigl, Otto M. Friedrich, Jr. and Arwin A. Dougal, "Mach-Zehnder Optical Interferometry of Laser-Induced Discharges in High Pressure Gases," 19th Annual Southwestern IEEE Conference and Exhibition, Dallas, Texas, April 19-21, 1967.

6. R. B. Allen, T. F. Whittaker and Arwin A. Dougal, "Laser Oscillations on Electronic Transitions in Neutral N_2 and CO," 19th Annual Southwestern IEEE Conference and Exhibition, Dallas, Texas, April 19-21, 1967.

B. Lectures Presented:

1. Arwin A. Dougal, "Fusion Plasma, Laser and Coherent Electro-Optics Research," Fifth Annual Industrial Associates Conference, Inn of the Six Flags, Dallas-Ft. Worth, Texas, February 1, 1967.

2. Arwin A. Dougal, "Fusion Plasma, Laser and Coherent Electro-Optics Research," Fifth Annual Industrial Associates Conference, Sheraton-Lincoln Hotel, Houston, Texas, February 3, 1967.

*Consolidates all papers presented, lectures, and publications by faculty and staff.

C. Publications:

1. Arwin A. Dougal and William H. Carter, "Field Range and Resolution in Holography," Journal of the Optical Society of America, 56, pp. 1754-1759, 1966.

2. Frederic Weigl, Otto M. Friedrich, Jr. and Arwin A. Dougal, "Laser Illuminated Mach-Zehnder Interferometry of a Laser-Induced Plasma," Bulletin of the American Physical Society, II-12, p. 178, 1967 (ABSTRACT).

3. Marion O. Hagler and Arwin A. Dougal, "Resonant Faraday Rotation in a Magnetoplasma-Filled Optical Resonator," Bulletin of the American Physical Society, II-12, p. 192, 1967 (ABSTRACT).

4. Arwin A. Dougal and Dennis H. Gill, "Mechanisms for Laser-Induced Breakdown of Super-High Pressure Gases," Bulletin of the American Physical Society, II-12, p. 227, 1967 (ABSTRACT).

5. Frederic Weigl, Otto M. Friedrich, Jr. and Arwin A. Dougal, "Mach-Zehnder Optical Interferometry of Laser-Induced Discharges in High Pressure Gases," Record of the 1967 Southwestern IEEE Conference and Exhibition, p. 2-2-1, April 19-21, 1967.

6. R. B. Allen, T. F. Whittaker and Arwin A. Dougal, "Laser Oscillations on Electronic Transitions in Neutral N_2 and CO," Record of the 1967 Southwestern IEEE Conference and Exhibition, p. 5-1-1, April 19-21, 1967.

ILLUSTRATIONS

II. DETERMINATION OF POWER FLOW IN ION CYCLOTRON RESONANCE PLASMA HEATING

III. EXPERIMENTAL INVESTIGATION OF HYDROMAGNETIC WAVE PROPAGATION AT LOW MAGNETIC FIELDS

PROPAGATION AND DISPERSION OF HYDROMAGNETIC AND ION CYCLOTRON WAVES IN PLASMAS IMMERSED IN MAGNETIC FIELDS

Jimmy G. Melton and Nathan B. Dodge (Prof. Arwin A. Dougal)

I. INTRODUCTION

Damping of the ion cyclotron wave in a magnetic beach offers a promising method for heating plasma ions to extremely high temperatures. Since the process heats predominantly the ion constituents of the plasma, it can be used to heat the plasma ions directly, without relying on energy transfer through electron-ion collisions to achieve high ion temperatures.

It has been predicted[1] and verified[2] that power from an rf oscillator can be coupled to the ion cyclotron wave in a plasma with over 50% efficiency, the losses being primarily copper losses in the coupling arrangement. It has further been observed that about 90% of the energy in the wave can be transferred to the ions in the damping region.[3] Thus, the overall transfer of energy from the driving circuitry to ion energy can be made as high as 45% effective.

The primary objective of ion cyclotron resonance heating studies is to be able to heat the overall plasma as hot as possible with the power available. This involves optimizing each stage of the heating process with regard to the plasma temperature attained. The heating process may be regarded as having three stages: (1) coupling of energy to the plasma column, (2) transfer of the energy from the coupling region to the damping region via the ion cyclotron wave, and (3) the damping of the wave and the resulting ion heating.

A complete study of optimizing the heating process must include all of the losses and limitations involved. This includes energy lost due to the loss of particles, by anomalous diffusion or otherwise, energy lost due to undamped waves, or lost due to coupling to undesired waves, or heating limitations due to finite temperature effects. However, much is still to be learned about the energy which eventually heats the plasma ions.

The studies in progress, and described in this report, are concerned with determining heating efficiency of the ion cyclotron wave. Section II of the report presents analytical studies of the electromagnetic wave fields in the quasistatic approximation, with the objective of establishing means to measure experimentally the wave energy in the plasma wave. Also in Sec. II are experimental measurements performed to determine the rf power being coupled into the plasma. It has been found that little of the available power is being coupled into the plasma. Evidence is presented which relates the inefficient coupling to the "Mode X" coupling phenomena observed and effectively eliminated at other facilities.[4]

Section III presents the results from an experimental investigation of the waves which propagate below the ion cyclotron magnetic field. One of these waves has tentatively been identified as the "fast" hydromagnetic wave. It has been found that rf power can be coupled to this wave with about 10 times the efficiency as to the ion cyclotron wave.[5] It has also been found that the fast wave can be used to heat the plasma. This offers possibilities of preheating the plasma with the fast wave or of heating with the fast wave and the ion cyclotron waves simultaneously.

It was found that low magnetic field wave propagation occurs in "bands," or for separated ranges of magnetic field. It was also found that wave propagation and increased density occur together. This suggests that propagation of the wave at low fields increases the ionization.

Also presented in Sec. III are further observations on the generation of frequency harmonics when waves damp in the magnetic beach. It was reported in the previous semiannual report[6] that generation of harmonics of the wave frequency was found to be associated with wave propagation and damping in the magnetic beach region. Further investigations have revealed that a significant fraction of the wave energy may be converted to new modes which escape cyclotron damping.

Investigations are being continued into the flow of rf power in ion cyclotron wave propagation and damping. It is through studies such as these that the evaluation of the ultimate capability for plasma heating by ion cyclotron resonance absorption may be accomplished.

References for Section I

1. T. H. Stix, "Generation and Thermalization of Plasma Waves," Phys. Fluids 1, 4, 308 (1958).

2. R. M. Sinclair, K. Chung, M. A. Rothman, H. Yamato, and S. Yoshikawa, "Observations of Plasma Heating by Ion Cyclotron Waves in the Model C Stellarator," MATT-Q-22, April, 1965, pp. 1-12.

3. F. I. Boley, J. M. Wilcox, A. W. DeSilva, P. R. Forman, G. W. Hamilton, and C. N. Watson-Munro, "Hydromagnetic Wave-Propagation near Ion Cyclotron Resonance," Phys. Fluids 6, 925 (1963).

4. S. Yoshikawa, R. M. Sinclair, and M. A. Rothman, "Ion Heating in the Model C Stellarator," Proc. Int. Conf. on Plasma Physics and Controlled Nuclear Fusion Research, Culham, U.K., Sept. 1965, CN-21/121.

5. M. A. Rothman and K. Chung, "Heating of Plasma by the Fast Hydromagnetic Wave," MATT-Q-23, April, 1966, pp. 32-37.

6. N. B. Dodge, J. G. Melton, and A. A. Dougal, "Experimental Investigation of Nonlinear Plasma Phenomena," Semiannual Status Report No. 8 on NASA Grant NsG-353, University of Texas, Austin, Jan. 15, 1967, pp. 66-81.

II. DETERMINATION OF POWER FLOW IN ION CYCLOTRON RESONANCE PLASMA HEATING, Jimmy G. Melton and Nathan B. Dodge (Professor Arwin A. Dougal)

The central objective in plasma heating by ion cyclotron resonance heating is to maximize the amount of power being used to heat the plasma. In present-day experiments, the objective has become rather to optimize the plasma heating power. The problem becomes in practice twofold: to optimize the plasma heating process and to optimize the delivery of power to the heating process. Having achieved these, it is hoped that the overall process will be efficient enough to enable heating a large volume of plasma to thermonuclear temperature.

The ion cyclotron resonance heating process proceeds as follows: energy is coupled to the plasma column from a radio frequency source operating at or near the ion cyclotron frequency of the plasma. Some of this energy goes into the ion cyclotron wave, which propagates for $\omega < \Omega_i$, where Ω_i is the ion cyclotron frequency, $\Omega_i = \frac{ZeB_0}{m_i}$. The ion cyclotron wave is then made to damp via the ion cyclotron damping process by making $\omega = \Omega_i$. As the wave damps, it delivers its energy to the ions present, which then thermalize through collisions.

From this brief description it can be seen that there are three phases to be considered in optimizing plasma heating; (1) the coupling of energy into the ion cyclotron wave, (2) the delivery of energy by the wave to the damping region, and (3) the transfer of energy from the wave to the ions of the plasma. Each of these three phases must be adjusted to yield maximum plasma heating for the input power available.

Figure II-1 is a simplified block diagram of power flow. It shows only the dominant features of power flow, omitting many of the details such as electron heating. The power from the rf source goes into ionizing and heating the plasma, into ohmic losses in the coupling device, and into the plasma. Of that part which goes into the plasma, the percentage going into ion cyclotron waves can be made quite large by suitably adjusting the experimental conditions. The

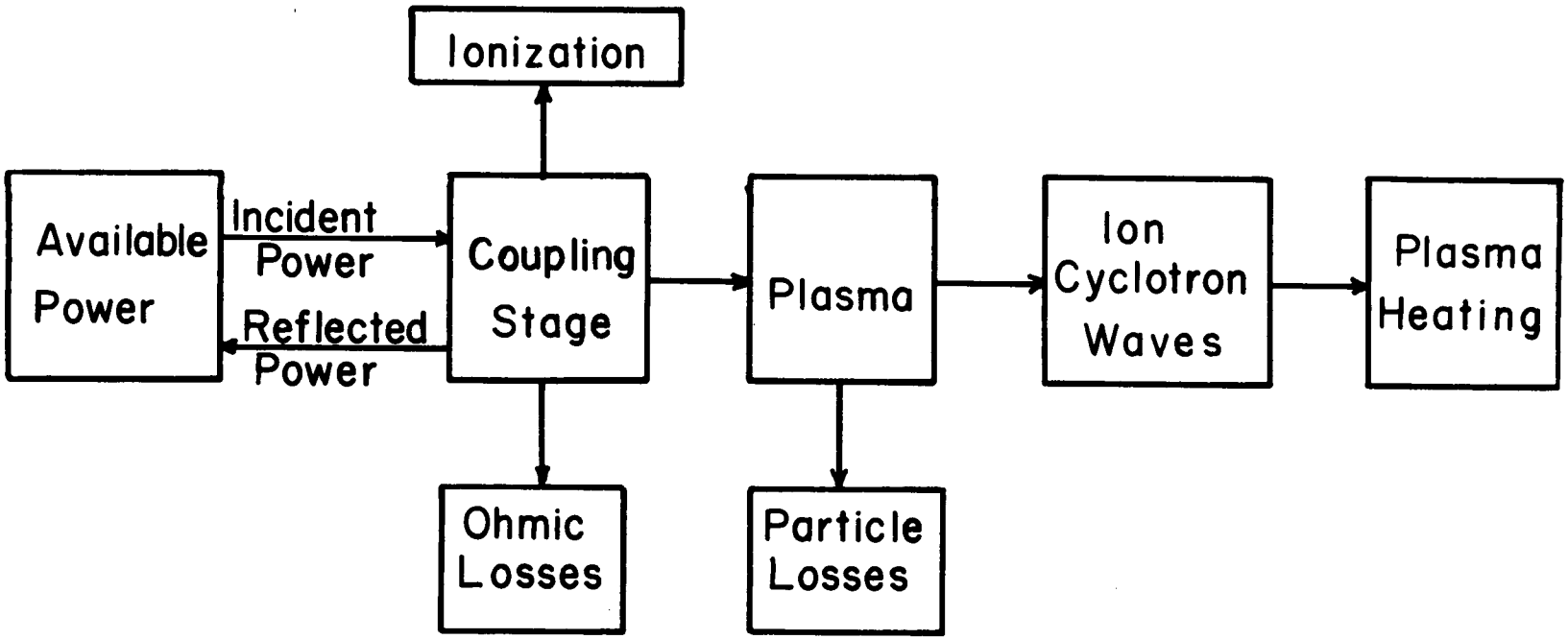

Fig. II-1. Simplified Block Diagram of Power Flow

power going into the plasma can be determined experimentally from measurements of incident and reflected power and from tuning conditions. In some cases the percentage of power going into ion cyclotron waves can also be determined by measurements of the magnetic signal associated with the wave. Similarly, measurements of the plasma diamagnetism can be used to determine plasma heating and temperature.

From measurements of this type, it is hoped that the efficiency of power transfer of each phase of the process can be determined. By comparing such measurements with results obtained from theoretical analysis, the optimum conditions for plasma heating can be determined, which would then afford an overall evaluation of the ion cyclotron resonance heating method.

Such optimization studies can be carried out using medium-powered experiments with experimental arrangements which stress flexibility. The results thus obtained can then be tried on high-power experiments of less flexible design.

It is to this objective of optimizing each phase of power transfer that these studies are directed. Experimental techniques are being developed to measure the power at each step in the energy transfer process. Analytical studies are being conducted in support of these techniques.

Section II-A presents a derivation of the relations between the electric and magnetic field components for ion cyclotron waves in the quasistatic approximation. With these relations, one can theoretically determine the wave energy density and power flow of ion cyclotron waves from measurements on the electric and magnetic fields of such waves.

A. Quasistatic Wave Field Amplitudes

At the present time, the wave coupling phase of ion cyclotron resonance heating experiments is relatively well understood. Several analyses[1,2] of the wave coupling process, in different approximations and varying degree of detail, have found fairly good agreement with experiment. There remains,

however, one aspect of experimental measurements on coupling efficiency which needs to be performed with more accuracy. Since not all of the power going into the plasma goes into the ion cyclotron wave, it is necessary to measure the energy flux of the wave in order to know how much was coupled into the plasma in some form other than ion cyclotron waves. Such measurements of the energy in the wave require quantitative measurements of the wave field amplitudes and a knowledge of the local plasma conditions for the measurement position. This section presents the relationships which exist between all six of the wave magnetic and electric field components in the quasistatic approximation (which seems to be valid for the conditions of the laboratory plasma under consideration).

The electric field of a wave in the plasma is given by the solutions of the wave equation

$$\nabla \times (\nabla \times \vec{E}) + \frac{\omega^2}{c^2} \overleftrightarrow{K} \cdot \vec{E} = 0$$

which satisfy the boundary conditions. A similar relation holds for the magnetic wave field $\vec{B}$. Here $\overleftrightarrow{K}$ is the effective dielectric tensor of the plasma.

For a cylindrical cold plasma of radius a and dielectric constant $\overleftrightarrow{K}$, the field parallel to a constant confining field $B_o \hat{z}$, are given by,[3]

$$E_z(r,z,t) = \sum_m \frac{\omega K_1' A_m}{k_m K_2' K_3'} \left[\beta_{1m} J_o(\nu_{1m} r) + \tau_m \beta_{2m} J_o(\nu_{2m} r) \right] e^{i(k_m z - \omega t)}, \qquad \text{(II-1a)}$$

$$B_z(r,z,t) = \sum_m A_m \left[J_o(\nu_{1m} r) + \tau_m J_o(\nu_{2m} r) \right] e^{i(k_m z - \omega t)} \qquad \text{(II-1b)}$$

The transverse fields can be expressed in terms of the longitudinal fields

$$E_\theta(r,z,t) = \sum_m (i\omega A_m) \left[\frac{J_1(\nu_{1m} r)}{\nu_{1m}} + \tau_m \frac{J_1(\nu_{2m} r)}{\nu_{2m}} \right] e^{i(k_m z - \omega t)} \qquad \text{(II-1c)}$$

$$B_\theta(r,z,t) = \sum_m \left(\frac{-i K_1' A_m}{k_m K_2'}\right)\left[\beta_{1m}\frac{J_1(\nu_{1m}r)}{\nu_{1m}} + t_m\beta_{2m}\frac{J_1(\nu_{2m}r)}{\nu_{2m}}\right] e^{i(k_m z-\omega t)} \tag{II-1d}$$

and

$$E_r(r,z,t) = \sum_m \left(\frac{-i\omega A_m}{K_2'}\right)\left[(\gamma_m+\nu_{1m}^2)\frac{J_1(\nu_{1m}r)}{\nu_{1m}} + t_m(\gamma_m+\nu_{2m}^2)\frac{J_1(\nu_{2m}r)}{\nu_{2m}}\right] e^{i(k_m z-\omega t)} \tag{II-1e}$$

$$B_r(r,z,t) = \sum_m (-i k_m A_m)\left[\frac{J_1(\nu_{1m}r)}{\nu_{1m}} + t_m\frac{J_1(\nu_{2m}r)}{\nu_{2m}}\right] e^{i(k_m z-\omega t)} \tag{II-1f}$$

In the above relations, only circularly symmetric modes are considered. k_m is the longitudinal wavenumber for the m^{th} mode, ν_m is the transverse wavenumber, and γ_m and $\beta_{1,2m}$ are given by

$$\gamma_m = k_m^2 - K_1' \tag{II-2a}$$

$$\beta_{1,2m} = \gamma_m - \frac{K_2'^2}{K_1'} + \nu_{1,2m}^2 \tag{II-2b}$$

and $K_{ij}' = \frac{\omega^2}{c^2} K_{ij}$ where the K_{ij} are the elements of the customary dielectric tensor $\overleftrightarrow{K}$ for the cold plasma in a magnetic field,

$$K = \begin{pmatrix} K_1 & K_2 & 0 \\ -K_2 & K_1 & 0 \\ 0 & 0 & K_3 \end{pmatrix} \tag{II-3a}$$

The elements are given by

$$K_1 = 1 - \frac{\omega_{pi}^2}{\omega^2-\Omega_i^2} - \frac{\omega_{pe}^2}{\omega^2-\Omega_e^2} \tag{II-3b}$$

$$K_2 = -i\left[\frac{\Omega_i}{\omega}\frac{\omega_{pi}^2}{\omega^2-\Omega_i^2} + \frac{\Omega_e}{\omega}\frac{\omega_{pe}^2}{\omega^2-\Omega_e^2}\right]$$

$$K_3 = 1 - \frac{\omega_{pi}^2}{\omega^2} - \frac{\omega_{pe}^2}{\omega^2} \qquad \text{(II-3b)}$$

A_m is the coefficient of the m^{th} mode, τ_m adjusts boundary conditions,

$$\tau_m = -\frac{\nu_{2m}}{\nu_{1m}}\frac{J_1(\nu_{1m}a)}{J_1(\nu_{2m}a)}$$

The boundary condition equations are solved simultaneously with the dispersion relation

$$\gamma^2 + K_2'^2 + \gamma\nu^2 + \frac{\nu^2 K_1'}{K_3'}\left(\gamma - \frac{K_2'^2}{K_1'} + \nu^2\right) = 0 \qquad \text{(II-4)}$$

to obtain ν_1^2 and ν_2^2. However, to solve the problem in its general form requires numerical computation.

The problem can be simplified considerably by suitable approximation to yield a dispersion relation with only one ν^2 solution. In the quasistatic approximation, in which we are interested, ν^2 is large, and

$$\frac{\nu^2}{K_3'} >> 1.$$

In this approximation, K_2' may be neglected so that, by taking $\tau_m = 0$, which is important only near the boundaries, one can derive the following field relations,

$$\frac{B_r}{E_\theta} = -\frac{k_\parallel}{\omega}, \quad \frac{B_z}{E_\theta} = \frac{k_\perp}{\omega}, \quad \frac{B_\theta}{E_r} = \frac{K_1'}{\omega k_\parallel} \qquad \text{(II-5a)}$$

One may also deduce

$$\frac{E_z}{B_\theta} = \frac{\omega}{k_\perp}\left(\frac{k_\parallel^2}{K_1'} - 1\right). \qquad \text{(II-5b)}$$

The above relations are sufficient to determine each of the wave field components in terms of theoretically measurable quantities and other field components. However, it is also possible to express each field component in terms of one of the others; for instance,

$$E_\theta = -\frac{K_2'}{\nu^2} E_r \qquad B_r = \frac{k_\parallel}{\omega}\frac{K_2'}{k_\perp^2} E_r$$

$$E_z = \left(\frac{k_\parallel}{k_\perp} - \frac{K_1'}{k_\perp k_\parallel}\right) E_r \qquad B_\theta = \frac{K_1'}{\omega k_\parallel} E_r \qquad \text{(II-6)}$$

$$B_z = -\frac{K_2'}{\omega k_\perp} E_r$$

Expressed in this way, within the limits of the approximation, i.e. $\nu^2/K_{ij}' \gg 1$, it is seen that E_r is the dominant electric component, with both E_z and E_θ being much less than E_r, whereas $B_\theta \gg B_z > B_r$ holds for the magnetic field components.

Having expressed the wave field components in this form, it is now possible to propose a method of determining wave power flow from magnetic probe measurements of the wave. The method depends on the quasistatic approximation being valid (though if it were not valid, wave field relations could still be derived which would be different from those presented above), that the pertinent plasma parameters are known (density and magnetic field), and, most importantly, that no more than one transverse mode exists and the wavelength parallel to the magnetic field can be determined.

If these conditions are met, then the transverse wavenumbers ν may be determined from the relation,

$$B_z/B_r = -\nu/k_\parallel \qquad \text{(II-7)}$$

Knowing ν, the wave field relations can be used in Poynting's theorem for the plasma, as presented in Ref. 4, to determine the wave energy content for quasistatic ion cyclotron waves. If the quasistatic condition is not a good approximation for the plasma, a similar analysis will yield the appropriate field

relation to be used. The critical assumption, however, is that the wave is composed of a single transverse mode. If this is not the case, other means must be used to determine wave energy density.

B. Experimental Measurements of Power Coupling

The experiment performed on power coupling to the plasma consisted of measuring incident and reflected power to the plasma, together with simultaneous measurements of the current flowing in the Stix coil, first with no gas and then with plasma in the system. Analysis of the data reveals the power being lost to the resistance of the coil, and the combined power going into the coil resistance and into the plasma.

The experimental arrangement is shown in Fig. II-2. It consists of a Pyrex discharge tube 6.25 cm in outside diameter located in a solenoidal magnet system. The magnetic field is adjustable up to 10 kG. The field configuration has modest 10% mirrors on each end, a 40 cm region where the field is uniform to $\pm 1/2\%$, and a "magnetic beach" of 50 cm length, which has a minimum field of 82% of that in the uniform region. The distance between mirror peaks is 130 cm. The magnetic field configuration is shown in Fig. II-3.

Preionization of the deuterium gas is provided by either or both of two rf systems; (1) a 40 kW oscillator at 7.5 MHz capacitively coupled to the plasma through two copper straps at the mirror peaks, and (2) a 1.5 kW rf amplifier at 21.3 MHz connected between internal electrodes located at the ends of the system outside the mirrors.

The main rf unit is a 30 kW pulsed amplifier at 5.8 MHz which is connected through directional couplers and a tuning box to a Stix coil surrounding the discharge tube in the uniform region of the magnetic field. A Rogowsky belt for measuring coil current is located around the feed strap to the Stix coil.

The Stix coil is center-fed, with four phase-reversed sections of three turns each. It has a wavelength of 16 cm. Electrostatic shielding is provided by an ungrounded "squirrel cage" Faraday shield, consisting of a number of axial strips of 0.060" copper 3/8" wide bonded between mylar sheets.[5]

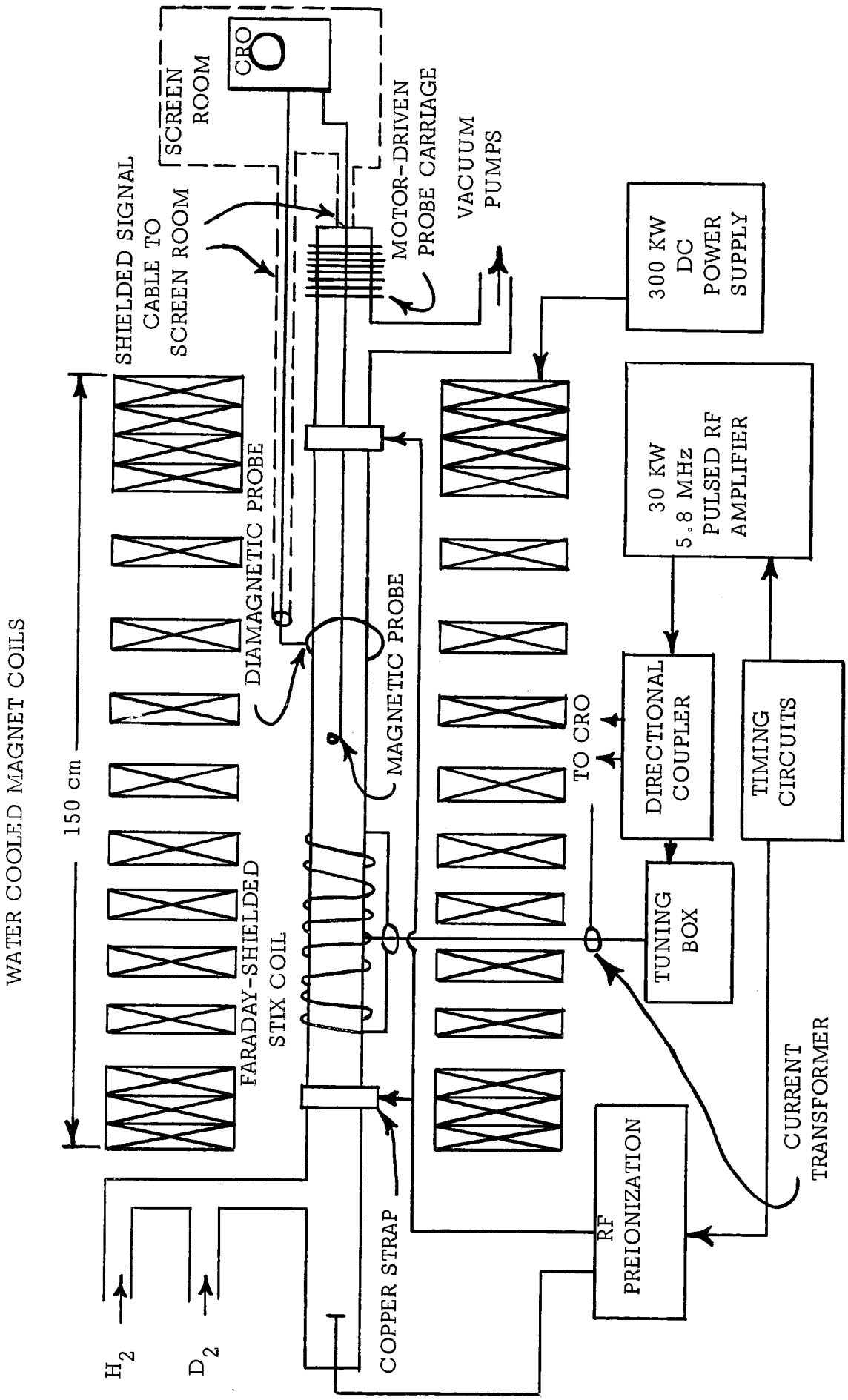

Fig. II-2 Block Diagram of ICRH Experiment

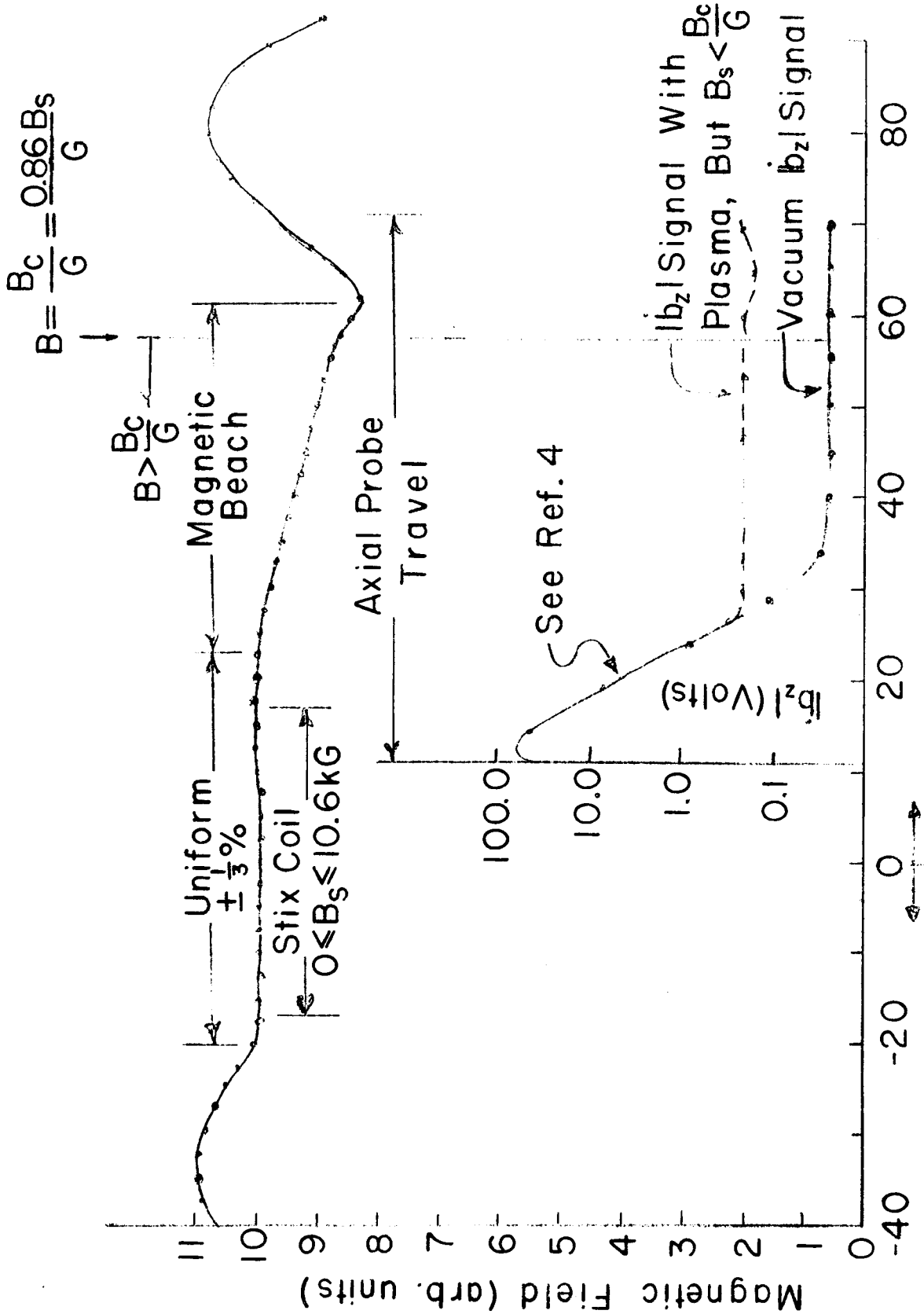

Fig. II-3 Magnetic Field Configuration and $\dot{b}_z$ Pick-up

On the beach end of the discharge tube, a movable probe carriage provides access to the plasma for magnetic probes by means of a re-entry glass tube--bellows arrangement. Also located in the beach region is a diamagnetic loop around the outside of the discharge tube to provide a measure of the plasma density-transverse temperature product. At the time this experiment was performed the diamagnetic probe was not calibrated and was used only to provide a relative measure of plasma heating. Similarly, an 8-mm microwave interferometer has been used to measure densities from $2 \times 10^{11} cm^{-3}$ to $8 \times 10^{11} cm^{-3}$, although density measurements were not performed at the same time the power input measurements were made.

The input power experiment consisted of simultaneously recording incident power, reflected power, and Stix coil current, first with no gas in the system, and then with plasma. Magnetic probe signal ($\dot{b}_z$) and diamagentic probe signal were monitored to verify wave propagation and plasma heating.

The effective plasma resistance can be calculated from power and current measurements for the vacuum and plasma cases by means of the relation

$$R = R_c + R_p = (P_i - P_r)/I_c^2 \qquad \text{(II-8)}$$

where R_c is the Stix coil resistance, R_p is the effective plasma resistance, P_i is incident power, P_r is reflected power, and I_c is the Stix coil current. (For further details see Ref. 5.)

Figure II-4 shows the data obtained. For these oscillographs, the preionization was not used, such that the plasma was created in the middle of the main ICRH pulse. Data obtained are plotted in Fig. II-5.

The data reveal that only a small percentage (less than 10%) of the power is going into the plasma. This point is considered later in the report, with a possible explanation and remedy.

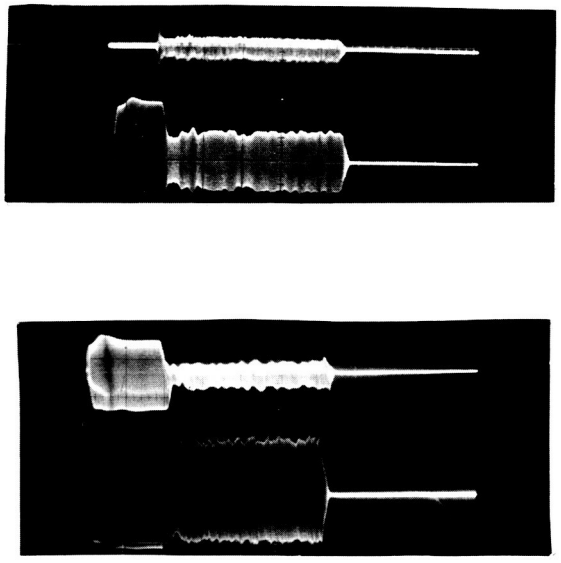

A. Wave Magnetic Signal
0.2 v/cm

B. Stix Coil Current
about 100 amp/cm

C. Reflected Power
1 v/cm

D. Incident Power
1 v/cm

Gas Pressure: 0.4 millitorr hydrogen
Magnetic Field: 6250 gauss

Fig. II-4. Oscillographs of Incident and Reflected Power and Stix Coil Current.

The time scale on these oscillographs is 200 μs/cm. Before 400 μsec, there is little or no plasma present. Breakdown occurs at 400 μsec.

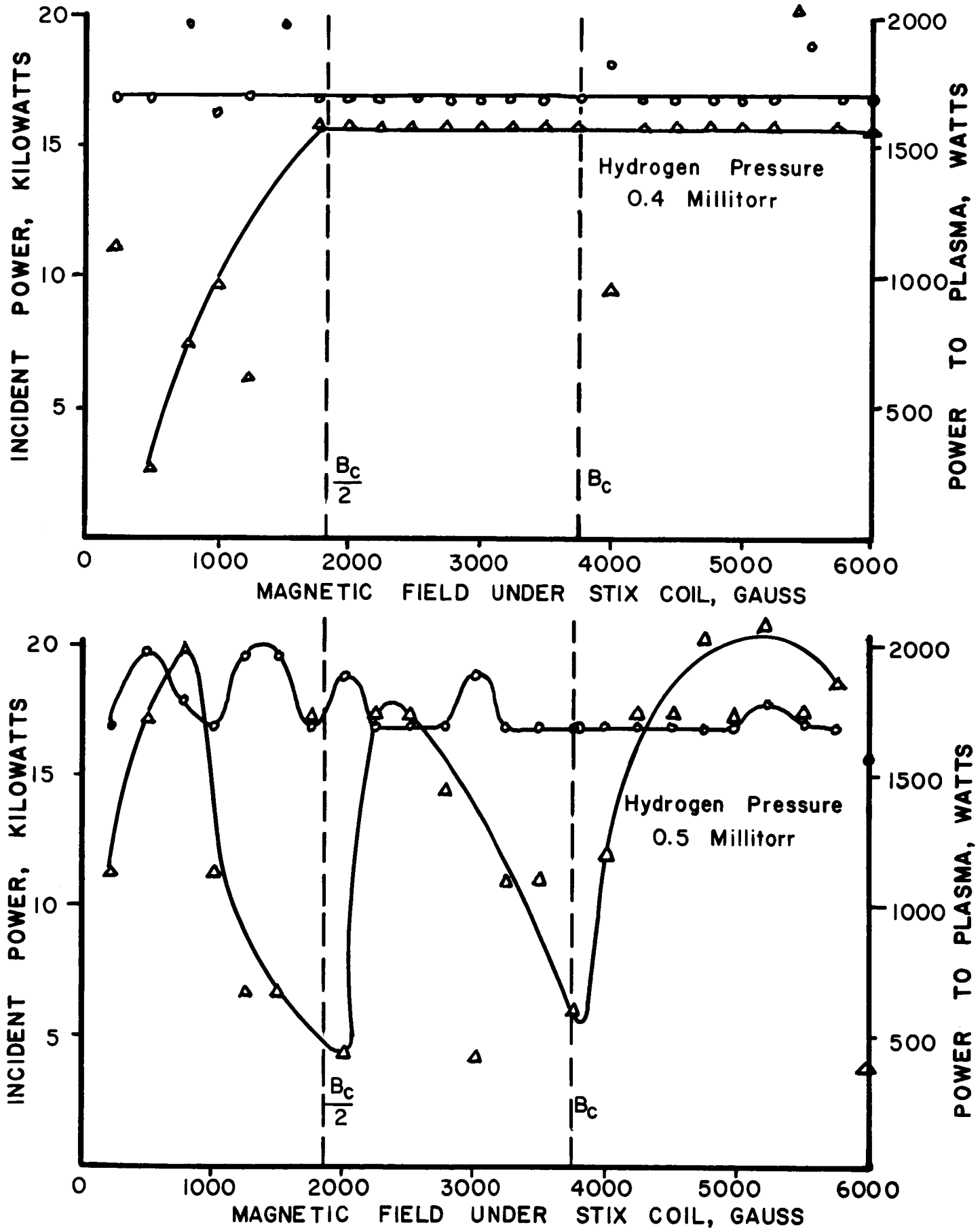

FIG. II-5 POWER COUPLING TO PLASMA vs MAGNETIC FIELD

In order to determine how much of the input power was appearing in the ion cyclotron wave, a magnetic probe (b_z) was used to measure wave magnetic signal amplitude and to determine the axial wavelength for the waves. The wavelength measurements were performed by measuring phase shift of the wave as the magnetic probe was moved through the beach region. To measure phase shift, the Stix coil current, measured by the Rogowsky belt, was used as a phase reference, and displayed on the same dual beam oscilloscope as the wave magnetic signal. Typical data are shown in Fig. II-6.

No phase shift was observed for the range of conditions investigated. It is estimated that the axial wavelength would have to be greater than 200 cm before no phase shift could be detected by this method. $\lambda_{\parallel} = 200$ cm implies a $k_{\parallel}$ of $\pi \times 10^{-2}$ or $k_{\parallel}^2 \approx 10^{-3}\,\mathrm{cm}^{-1}$. To determine if the phase measurements are possible, the curve of Fig. II-7 was plotted, using the cold plasma dispersion relation for the ion cyclotron wave,

$$c^2 k_{\parallel}^2 = \left(\frac{\omega_{pi}^2 \omega^2}{\Omega_i^2 - \omega^2} - \frac{c^2 k_{\perp}^2}{2}\right) \pm \left[\left(\frac{\omega_{pi}^2 \omega^2}{\Omega_i^2 - \omega^2} - \frac{c^2 k_{\perp}^2}{2}\right)^2 + \frac{\omega_{pi}^2}{\omega_{pe}^2} \frac{\omega^2}{(\Omega_i^2 - \omega^2)} \left(c^4 k_{\perp}^4 + c^2 k_{\perp}^2 \omega_{pe}^2 - \frac{\omega_{pi}^2 \omega^2 \omega_{pe}^2}{\Omega_i^2}\right)\right]^{1/2} \quad \text{(II-9)}$$

A value of $k_{\perp}^2 = 1.0$ corresponds roughly to the lowest order radial mode. For $k_{\perp}^2 = 1.0$, and a density of greater than $10^{11}\,\mathrm{cm}^{-3}$ it is seen that $k_{\parallel}^2$ is on the order of 10^{-1}, or the axial wavelength $\lambda_{\parallel}$ is 20 cm.

In order for the wavelength to be as long as the phase shift measurements indicate, either the density must be much less than $10^{11}\ \mathrm{cm}^{-3}$, or the magnetic probe is responding either to noise or to a long wavelength "standing-wave" oscillation. Since it is not yet settled which situation exists, further investigations will be conducted to resolve the question of wavelength.

During the experiment to determine wavelength, it was observed that the wave magnetic signal (b_z) can possess a very complex fine structure. This fine structure at times became quite pronounced. Typical fine structures are shown in Fig. II-8 on three different time scales. There are oscillations at 25 MHz,

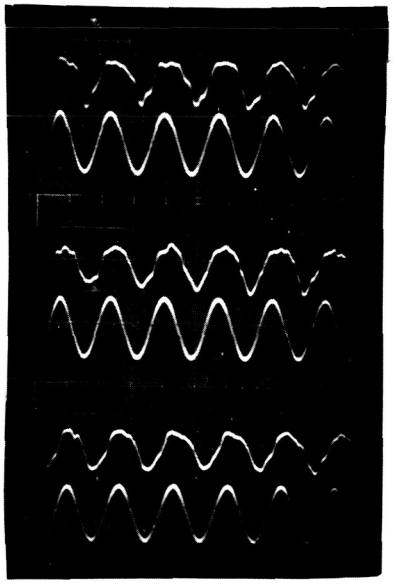

Phase-Shift Measurements

Upper trace: Wave magnetic signal
0.5 v/cm.

Lower trace: Stix Coil Current
@ 50 amp/cm.

Time scale: 0.1 μsec/cm.

Conditions: p = 0.3 mT of D_2
B_0 = 4100 gauss

Top pair: Magnetic probe located
at Z = 51 cm.

Middle pair: Z = 41 cm.

Bottom pair: Z = 31 cm.

Fig. II-6. Determination of Axial Wavelength of 2nd Harmonic Ion Cyclotron Waves.

Wavelength is measured by determining the phase-shift between the current in the Stix Coil and the magnetic probe b_z.

The probe position is indicated by its distance Z from the center of the Stix Coil.

The axial wavelength of the Stix Coil is 16 cm. No phase shift through the plasma is evident in these oscillographs.

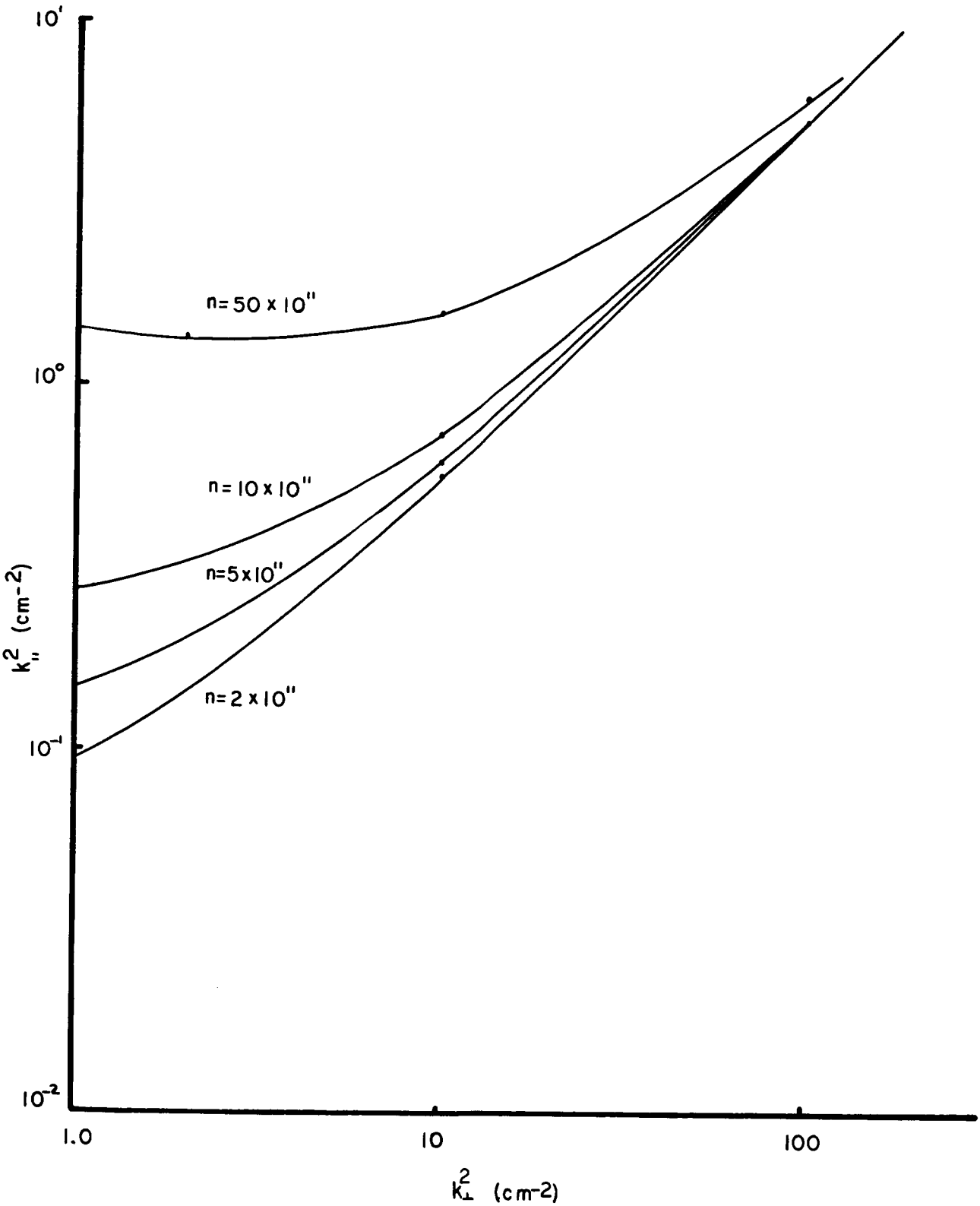

Fig. II-7. Axial Wave Number vs Transverse Wave Number for Cold Plasma Ion Cyclotron Wave, with Electron Inertia Effects.

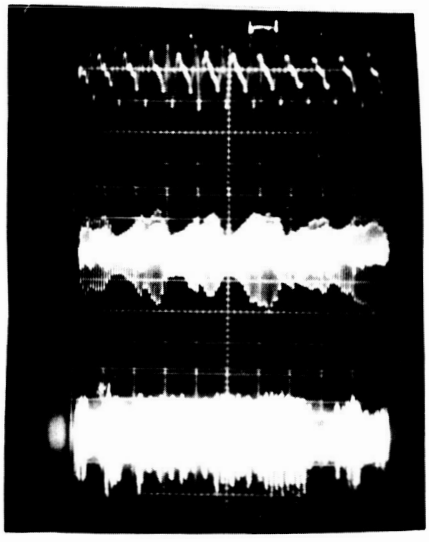

Wave Magnetic Probe Signal

(1.) 0.2 μsec/cm

(2.) 2.0 μsec/cm

(3.) 20 μsec/cm

Conditions: $p = 0.3$ mT in D_2
$B_o = 4500$ gauss
$Z^o = 45$ cm

Fig. II-8. Fine Structure on Wave Magnetic Signal.

Showing the shape of the wave magnetic signal on successively slower time sweeps for conditions which give a propagating wave.

Probe is positioned 45 cm from the center of the Stix Coil, in the magnetic beach region.

The top oscillograph shows oscillations at the driving frequency, 5.8 MHz, and at about 25 MHz.

The middle oscillograph shows oscillations at about 280 KHz.

The bottom oscillograph shows oscillations at about 30 KHz.

5.8 MHz (the driving frequency), 278 KHz, and about 30 KHz. Similar oscillations have been observed in other experiments[6] and previously on this experiment.[7] The cause and the nature of these oscillations is not known at present. It is interesting to note that the oscillations seem to be of the relaxation type.

C. Evidence of Non-resonant Coupling of Power to the Plasma

In the previous section it was noted that the power coupled to the plasma was lower than expected. Of greater significance is the observation that the power to the plasma does not peak near $B = B_c$. This suggests that the power is coupling to the plasma by some mechanism other than to the ion cyclotron wave.

Reports on experiments at other facilities have mentioned similar non-resonant coupling phenomena.[8] On the Model C Stellarator a similar occurrence of non-resonant coupling was remedied by improving the shielding of the E_z component Stix coil. The mechanism which has been advanced for "Mode X," as it is called, is that the fringing E_z fields into the plasma accelerate the electrons along the magnetic field lines, so that the resulting space charge field drives the ions into the wall of the discharge tube. The significant improvement obtained by introducing a Faraday shield between the plasma and the Stix coil lends support to this mechanism.

In addition to the power input measurements, two observations suggest that "Mode X" is limiting the power to plasma waves in the present studies. The first is that plasma density measured by an 8-mm microwave interferometer is present even when no gas is in the system. The second is that the current drawn by the ionization vacuum pump increases when the system is pulsed several times in rapid succession. Both of these observations suggest there is a high particle influx rate from the tube wall during the ICRH pulse.

The apparent solution is to improving the present shielding arrangement of the Stix coil. An improved Faraday-shielded Stix coil has been designed and constructed and will be installed on the experiment. With the new coil in place, studies will be continued into the efficiency of coupling power into the ion cyclotron wave.

References for Section II

1. T. H. Stix, "Generation and Thermalization of Plasma Waves," Phys. Fluids, 1, 4, p. 308 (1958).

2. R. R. Woollett, "Energy Addition to an Atomic Hydrogen Plasma at Off-Resonant Conditions," NASA Technical Note TN D-2982, September, 1965.

3. D. G. Swanson, R. W. Gould, and R. H. Hertel, "Experimental Study of Compressional Hydromagnetic Waves," Phys. Fluids 7, 2, p. 269 (1964).

4. J. G. Melton and A. A. Dougal, "Theoretical Investigations of Quasi-static Ion Waves and Wave Energy Densities," S.S.R. No. 8 on NASA Grant NsG-353, pp. 34-50, January 15, 1967.

5. M. Kristiansen, J. G. Melton, F. C. Harris, N. B. Dodge and A. A. Dougal, "Experimental Investigation of Wave Coupling Structure," S.S.R. No. 6 on NASA Grant NsG-353, pp. 36-51 and pp. 20-26, January 15, 1966.

6. R. S. Pease, S. Yoshikawa and H. P. Eubank, "The Confinement of Plasma Heated by Ion Cyclotron Resonance in the C Stellarator," MATT-Q-23, p. 7, April, 1966.

7. M. Kristiansen, F. C. Harris, N. B. Dodge, J. G. Melton and A. A. Dougal, S.S.R. No. 5 on NASA Grant NsG-353, pp. 35-44, July 15, 1965.

8. S. Yoshikawa, M. A. Rothman and R. M. Sinclair, "Nonresonant Coupling of ICRH Power to C-Stellarator Plasmas," MATT-Q-22, pp. 28-35, April, 1965.

III. EXPERIMENTAL INVESTIGATION OF HYDROMAGNETIC WAVE PROPAGATION AT LOW MAGNETIC FIELDS, Nathan B. Dodge and Jimmy G. Melton (Professor Arwin A. Dougal)

Observations of wave propagation at very low magnetic fields have previously been reported[1] from this facility. The waves which have been seen at low magnetic fields ($B \lesssim 1000$G) have been referred to as the so-called "fast" hydromagnetic wave.[1] Since heating and enhanced ionization of plasma may occur during the "fast" wave propagation,[2,3] and since all hydromagnetic wave phenomena are of interest in the study of radio-frequency plasma heating, a study has been made of these low magnetic field wave phenomena, the initial results of which are reported here.

Part A of this section describes the behavior of the wave phenomena, including onset and attenuation characteristics, and sensitivity of the wave to neutral pressure and magnetic field. Plasma heating and electron density during the wave propagation are discussed in Part B. Part C extends the nonlinear frequency phenomena investigation initiated in the previous report period to the study of harmonic generation in low magnetic field waves. Part D consists of a discussion and interpretation of the three sections preceding, and Part E includes plans for completing the low field investigation and continuing the study of nonlinear plasma phenomena.

A. Hydromagnetic Wave Propagation at Low Magnetic Fields

At lower magnetic fields such that $\omega > \Omega_c$ ($B \lesssim 1.0$ kG) wave phenomena have been observed and reported.[1] These phenomena were taken to be due to the so-called "fast" hydromagnetic wave. Recent studies, considered here, confirm the existence of extensive wave propagation in one or more bands. Data presented here is confined to hydrogen.

The wave propagation depends rather sensitively on neutral gas pressure. At 0.3 mTorr, as seen in Fig. III-1, there is a gradual decay in wave magnetic signal, b_z, as the static magnetic confining field B_o is reduced. Low-field propagation ($B \lesssim 1000$ G) has not been observed below 0.3 mTorr.

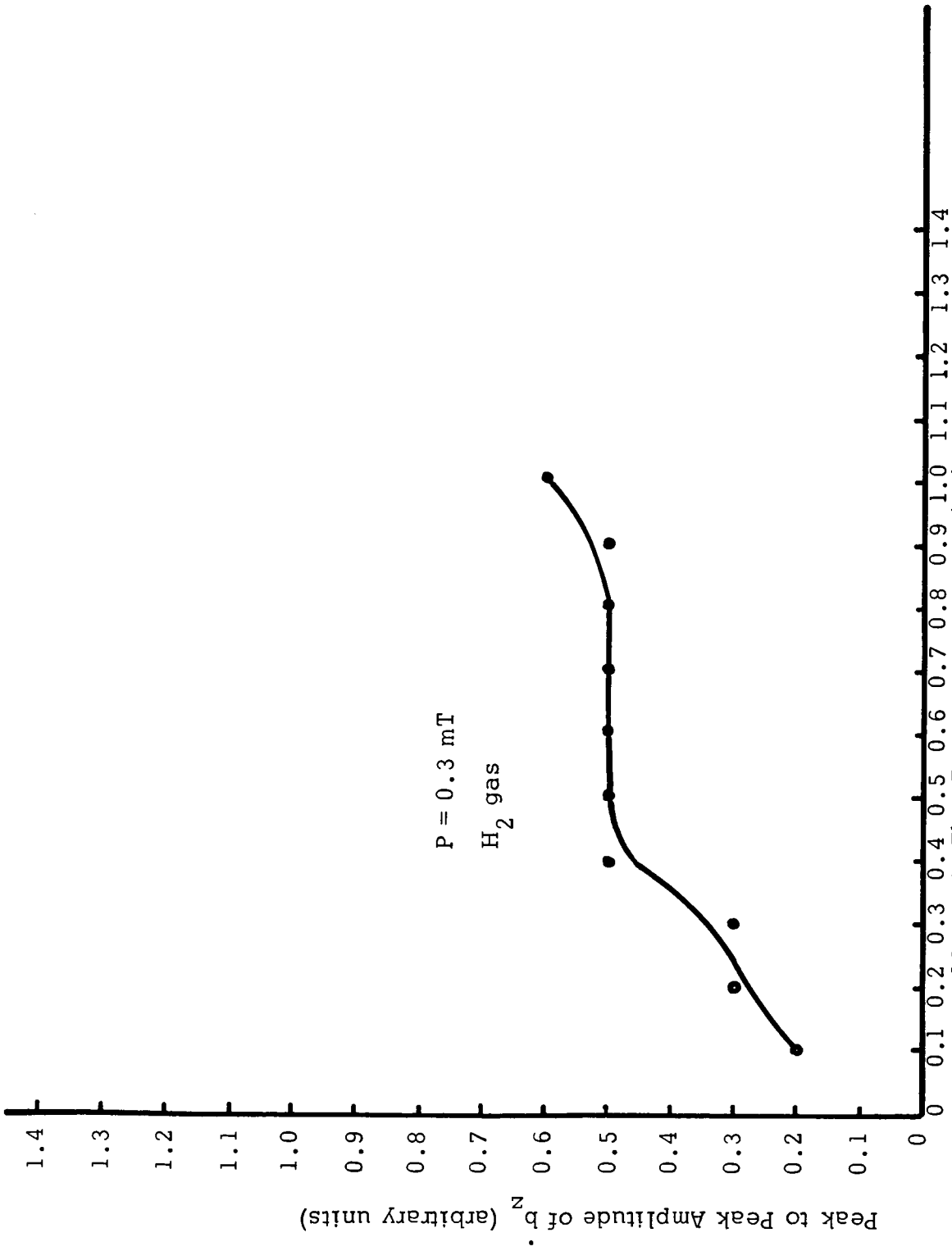

Fig. III-1. Wave Magnetic Signal ($\dot{b}_z$, p-p) at 0.3 mT.

Onset of propagation appears to occur normally at about 0.4 mTorr, around 500 G, as shown in Fig. III-2a. For comparison, $\dot{b}_z$ at 0.3 mTorr, 500 G is also shown in Fig. III-2b. Wave magnetic signal ($\dot{b}_z$) is ragged in the former figure, indicating that the conditions for propagation are marginal, at best. The wave appears to attenuate at 400 G, but again "tries" to propagate at 300 G, as in Fig. III-2c. There appears to be marginal propagation down to around 200G, but below this field the wave field gradually decreases until the wave appears to be cut off around 75 G, (Fig. III-2d).

The appearance of two fuzzily separated propagation bands is further illustrated by data taken at 0.5 mTorr. A plot of magnetic signal versus confining field reveals two fairly broad regions of propagation separated by a narrow, indistinct "stop-band" or region of signal attenuation, as shown in Fig. III-3. Again, there is a large amount of variation in the amplitude of $\dot{b}_z$, as indicated on the graph, in the propagation bands, so that evidently conditions are still near-marginal for propagation.

It is interesting that the "stop-band" appears to have narrowed somewhat from the band at 0.4 mTorr and is only about 50 to 100 G wide. The stop bands and propagation band retain the same configuration at 0.6 mTorr, but the stop band appears to be wider in this case, and the propagation band around 500 G seems somewhat wider. The trend continues at 0.7 mTorr.

Figure III-4 shows $\dot{b}_z$ versus B_o at 0.8 mTorr. The magnetic signal shows a broad peak around 500 G and two lesser peaks at 1 kG and 75 G, with broad stop bands of around 200 G between each one. There now appear to be three regions of propagation: (1) a weaker band below 100 G, (2) a broad, rather sharply defined band from 300 to about 650 G characterized by high amplitudes in $\dot{b}_z$, and (3) a band beginning at around 800-900 G. (Although this study was not carried out at magnetic fields above 1.0 kG, previous work indicates this band extends upward to about 2.2 kG at 0.8-0.9 mTorr in hydrogen gas.)

As implied by the above description, the stop bands extend from 100 to 300 G and from about 650 to 900 G. Studies so far have extended to 1.2 mTorr in

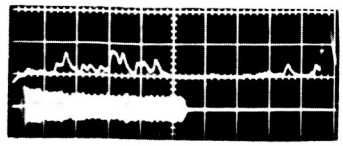

a. $\dot{b}_z$ (lower trace) Onset of propagation, first band.

p = 0.5 mT Z = 50 cm

H_2 gas Oscilloscope Sweep: 200 μsec/cm

B_o = 500 G

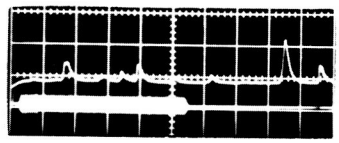

b. $\dot{b}_z$ (lower trace) No propagation.

p = 0.3 mT Z = 50 cm

H_2 gas Oscilloscope Sweep: 200 μsec/cm

B_o = 500 G

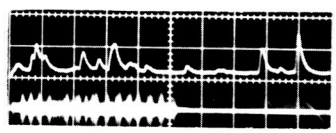

c. $\dot{b}_z$ (lower trace) Onset of propagation, second band.

p = 0.4 mT Z = 50 cm

H_2 gas Oscilloscope Sweep: 200 μsec/cm

B_o = 300 G

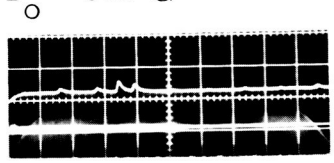

d. $\dot{b}_z$ (lower trace) Strong attenuation.

p = 0.4 mT Z = 50 cm

H_2 gas Oscilloscope Sweep: 200 μsec/cm

B_o = 75 G

Fig. III- 2. $\dot{b}_z$ During Propagation and Damping.
(Z = Distance to Center of Stix Coil)

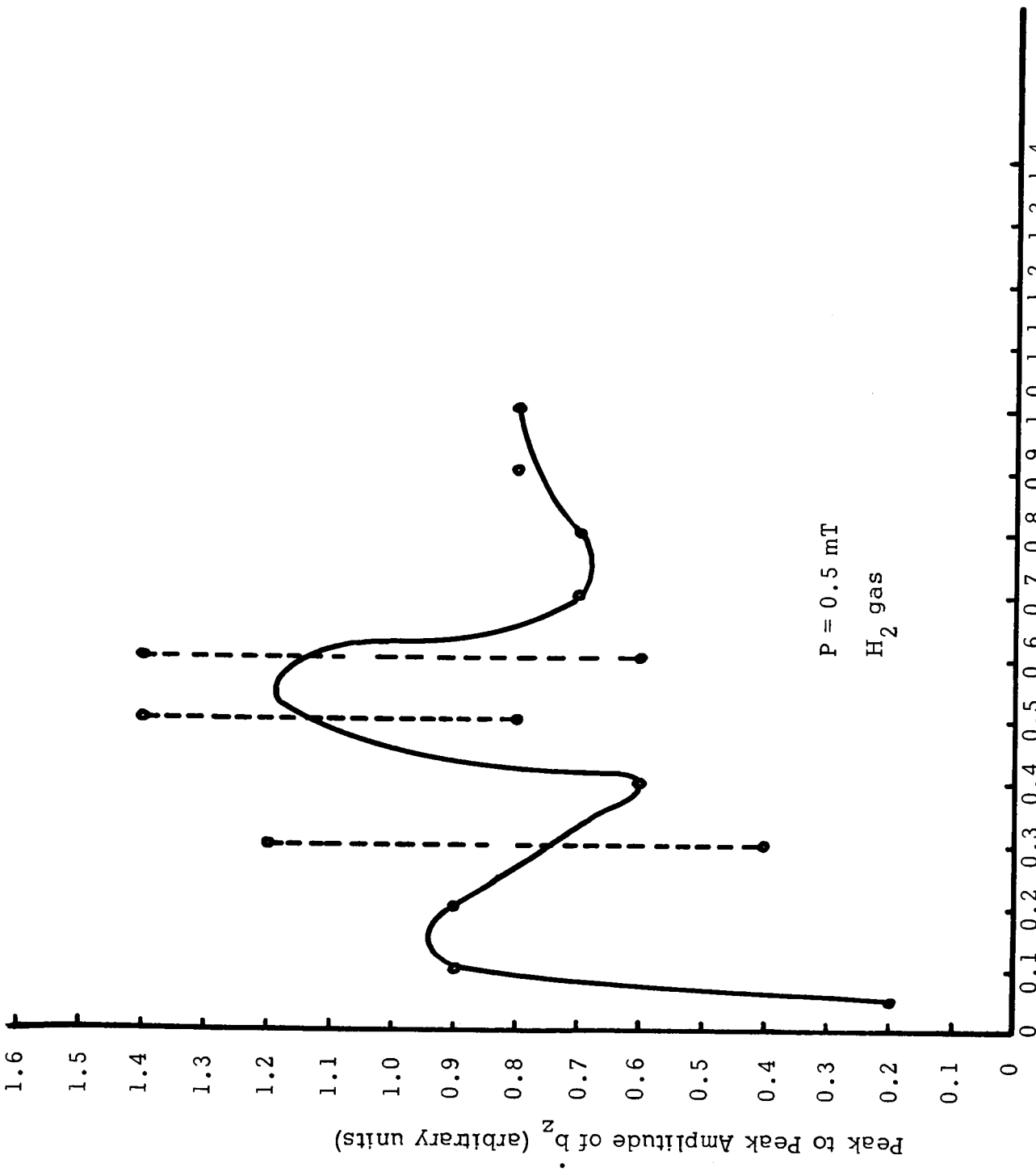

Fig. III- 3. Wave Magnetic Signal (b_z, p-p) at 0.5 mT.

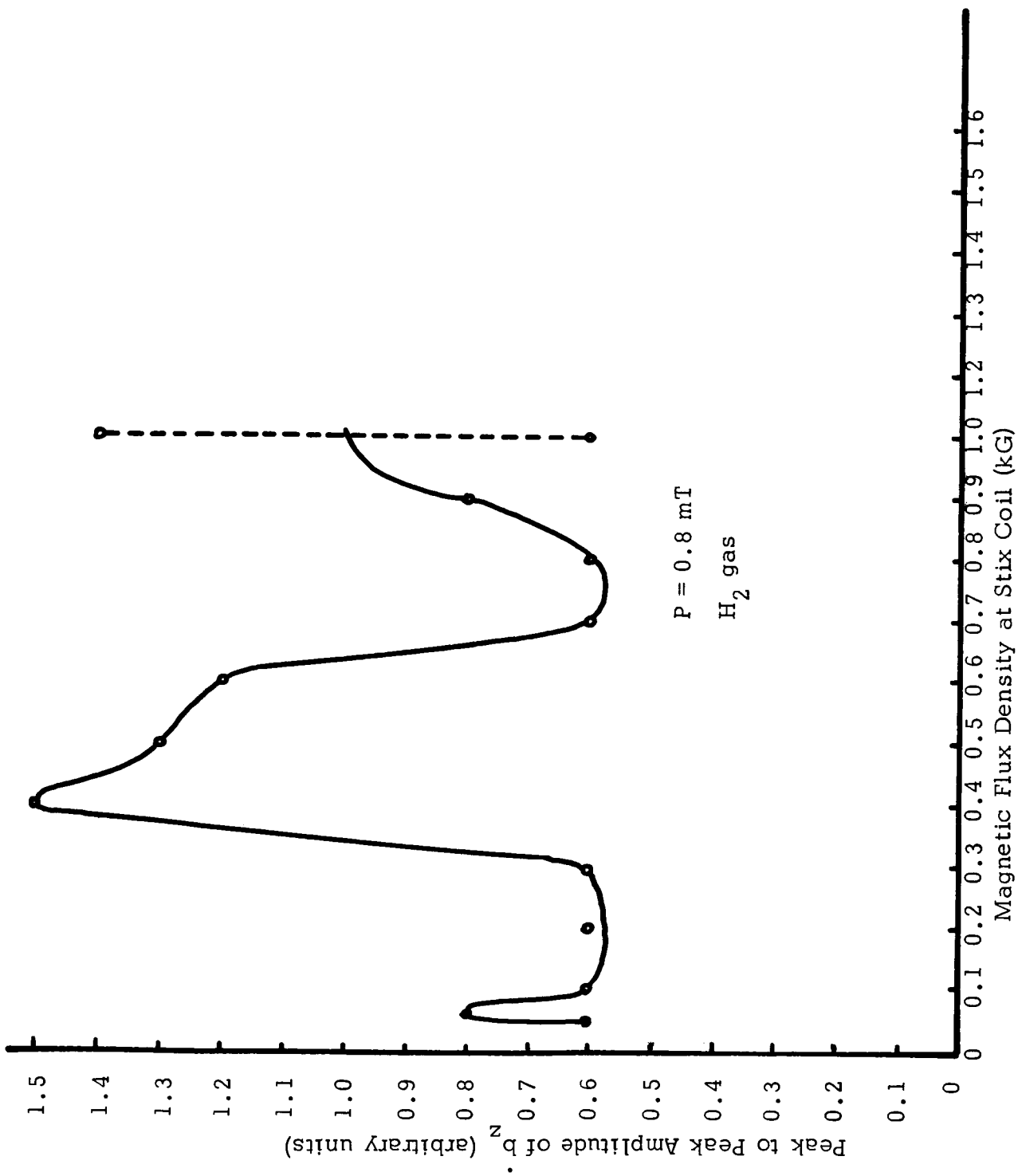

Fig. III-4. Wave Magnetic Signal ($\dot{b}_z$, p-p) at 0.8 mT.

hydrogen. Above 0.8 mTorr, there is a gradual disappearance of the lowest propagation band, while the central band broadens to include a range of 300-700 G at 1.2 mTorr. The lowest band is no longer in evidence at this highest pressure so far studied. The higher band is still in evidence, although it is about 500 G wide, extending from 800 or 900 G to 1.4 kG, indicating that a considerable narrowing of the band has taken place. (The upper limit of the band was verified from a previous study, as mentioned above for (3).)

Further data will be taken above 1.2 mTorr. The studies referred to above indicate, however, that above 1 or 2 mTorr a "flattening" of the peaks in the $\dot{b}_z - B_o$ curves and a "filling" of the valleys occurs. By about 10 mTorr, the $\dot{b}_z$ signal is more or less level over the range of B_o between 50 G and 1000 G. It is assumed that the reason for the gradual "smearing out" of wave phenomena above 1-2 mTorr is due to ion-neutral collisional effects, about which more will be said in Part D. At present, no investigations can be made below 50 G as this is the lower limit of the dc power supply.

B. Electron Density and Diamagnetic Signal Measurements of Low-Field Wave Phenomena

As has been reported previously,[4] a microwave interferometer has been installed which allows precise measurements of electron density. It is therefore possible to accurately monitor the percentage ionization in the laboratory plasma during the radio frequency heating cycle. With the provisions for measurement of diamagnetic signal already available,[5,6] it is a simple and straightforward procedure to calculate the relative change in ion temperature. Recall[5]

$$T_{e\perp} + T_{i\perp} = \left(\frac{1}{n}\right) \frac{V_s RC B_o}{NA \delta \mu_o \kappa} \qquad \text{(III-1)}$$

where $T_{e\perp}$ and $T_{i\perp}$ are the perpendicular electron and ion temperatures, respectively, n is the electron or ion density (assuming that $n_e = n_i = n$), V_s is the integrated diamagnetic signal, the RC product represents the time constant of the

integrator, B_o is the static magnetic confining field, N is the number of turns in the diamagnetic probe coil, A is the cross-sectional area of the plasma column, δ is the shape factor of the cross section, μ_o is the magnetic permeability (= $4\pi \times 10^{-7}$ hy/m), and κ is Boltzmann's constant (= 1.38×10^{-23} J/°K).

It may be seen that the integrated diamagnetic signal V_s is proportional to $(\frac{1}{B_o})$ by rewriting Eq. (III-1),

$$V_s = \frac{NA\delta\mu_o\kappa}{RC}\left[n(T_{e\perp}+T_{i\perp})\right]\left(\frac{1}{B_o}\right) \qquad \text{(III-2)}$$

Thus, as B_o is lowered, as in this experiment, V_s would normally increase, even though the $n(T_{e\perp} + T_{i\perp})$ product remained constant. In order that the variation of diamagnetic signal be strictly due to a change in n (ionization) or $T_{e\perp}$ and $T_{i\perp}$ (particle energy), the amplitude of V_s was corrected by multiplying each value of V_s by the corresponding value of B_o in kG, so that the term "diamagnetic signal" will subsequently refer to the $V_s B_o$ product, which varies only with density and temperature.

Since the microwave interferometer operates at very low power levels, and since the microwave equipment is operated in close proximity to the plasma environment, a large amount of radio noise contamination of the microwave signals was experienced. In order that difficulties in interpreting the composite signals would not arise the klystron reflector voltage was square-wave modulated so that the klystron in the microwave system was pulsed on and off, as seen in Fig. III-5. The difference in the "step" was measured to register the phase shift and therefore the plasma density.

Electron density is plotted versus B_o at 0.3 mTorr in Fig. III-6. It is interesting that the density falls very nearly as $\dot{b}_z$, and it was found that the correspondence between $\dot{b}_z$ and electron density was close in all the cases of interest. Figure III-7 depicts $\dot{b}_z$ and electron density plotted versus B_o at

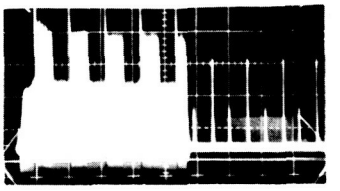

$p = 1.0$ mT $Z = 40$ cm

H_2 gas Oscilloscope Sweep: 200 μsec/cm

$B_o = 300$ G

Fig. III- 5. Typical Display of Microwave Interferometer with Square Wave Modulation of Reflector Voltage to Compensate for Noise Level.

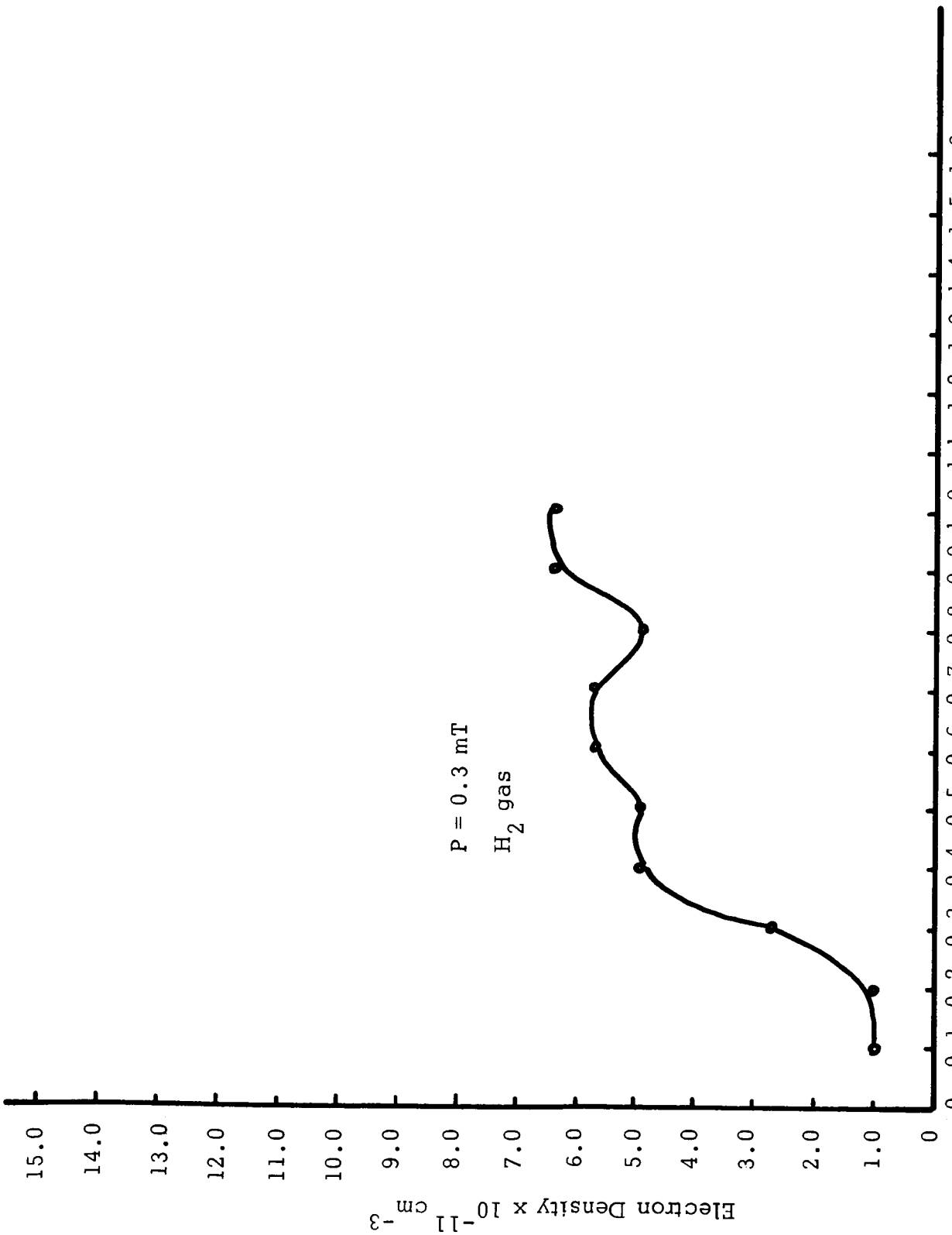

Fig. III- 6 . Electron Density at 0.3 mT.

0.8 mTorr (as mentioned earlier, all data mentioned in Section III was obtained for hydrogen gas).

Note that there is a close correspondence between the peaks in $\dot{b}_z$ and those in electron density. There is an especially close correpondence between the peak in $\dot{b}_z$ at around 500G (which is the center of the middle "propagation band") and the peak in electron density. This was also true at 0.5 mTorr and 1.0 mTorr, although the correspondence is not as close in the lower propagation band (50-100G). During strong propagation at 0.8 mTorr when the magnetic signal is almost triple the "stop-band" values (at $B_o \simeq$ 500G), the electron density has increased from a low of $5.5 \times 10^{11} cm^{-3}$ to $1.4 \times 10^{12} cm^{-3}$, which corresponds to an increase from about 1% to more than 2% in total ionization. Similar increases are evident at other neutral gas pressures for the propagation band centered at 500G. Typical plasma density signals during propagation and after wave attenuation are shown in Figs. III-8a and III-8b.

Diamagnetic probe measurements were made similar to those which have been previously reported in studies on ion cyclotron wave heating.[2,5,6] Because of the 360 Hz ripple inherent in the dc magnetic field power supply, the diamagnetic signal is passed through a high-pass filter before processing the oscilloscope plug-in amplifier. It is then amplified and integrated and the resulting signal displayed, a typical display being given in Fig. III-9.

A plot of diamagnetic signal versus B_o at 0.5 mTorr is shown in Fig. III-10. It is seen that $nKT_\perp$ decreases gradually above 700G and then sharply down to 50G. The decrease is regular, and there appears to be no peak in $nKT_\perp$ near the wave resonances, nor dip where the stop bands occur. Figure III-11 depicts $nKT_\perp$ at 1.0 mTorr and corresponding values for electron density and magnetic probe signal. Although there is a close correspondence between density and $\dot{b}_z$, $nKT_\perp$ gradually falls toward zero with no particular relation to the other curves. Idential behavior was registered throughout the entire 0.3 - 1.2 mTorr range, and the only close correspondence was found at 0.3 mTorr, where

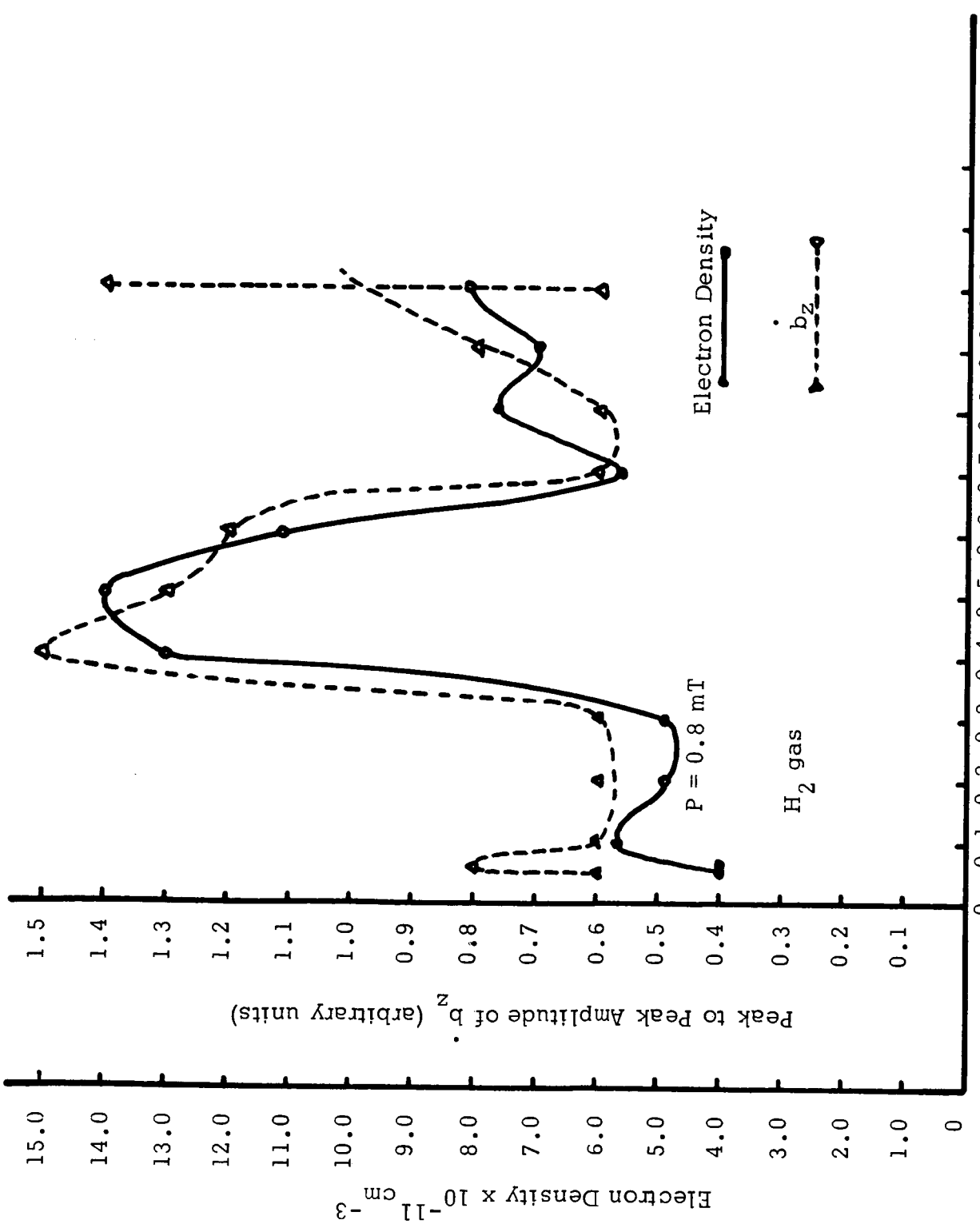

Fig. III- 7. Electron Density and b_z (p-p) at 0.8 mT.

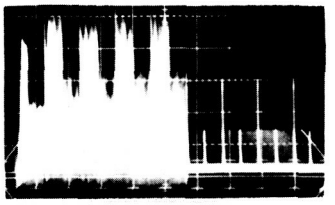

a.

p = 0.7 mT Z = 40 cm

H_2 gas Oscilloscope Sweep: 200 μsec/cm

B_o = 400 G

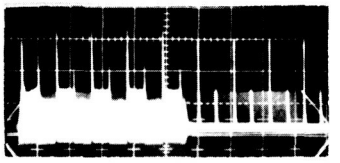

b.

p = 0.7 mT Z = 40 cm

H_2 gas Oscilloscope Sweep: 200 μsec/cm

B_o = 50 G

Fig. III- 8. Electron Density Signal from Microwave Interferometer during Propagation (a.) and Attenuation (b.) of Low Field Waves.

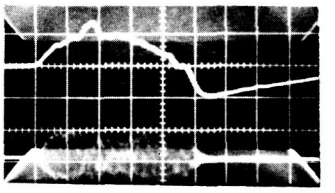

p = 0.8 mT
H_2 gas
B_o = 900 G

Z = 50 cm
Oscilloscope Sweep: 20 μsec/cm

Fig. III- 9 . Photograph of Typical Diamagnetic Signal Trace.

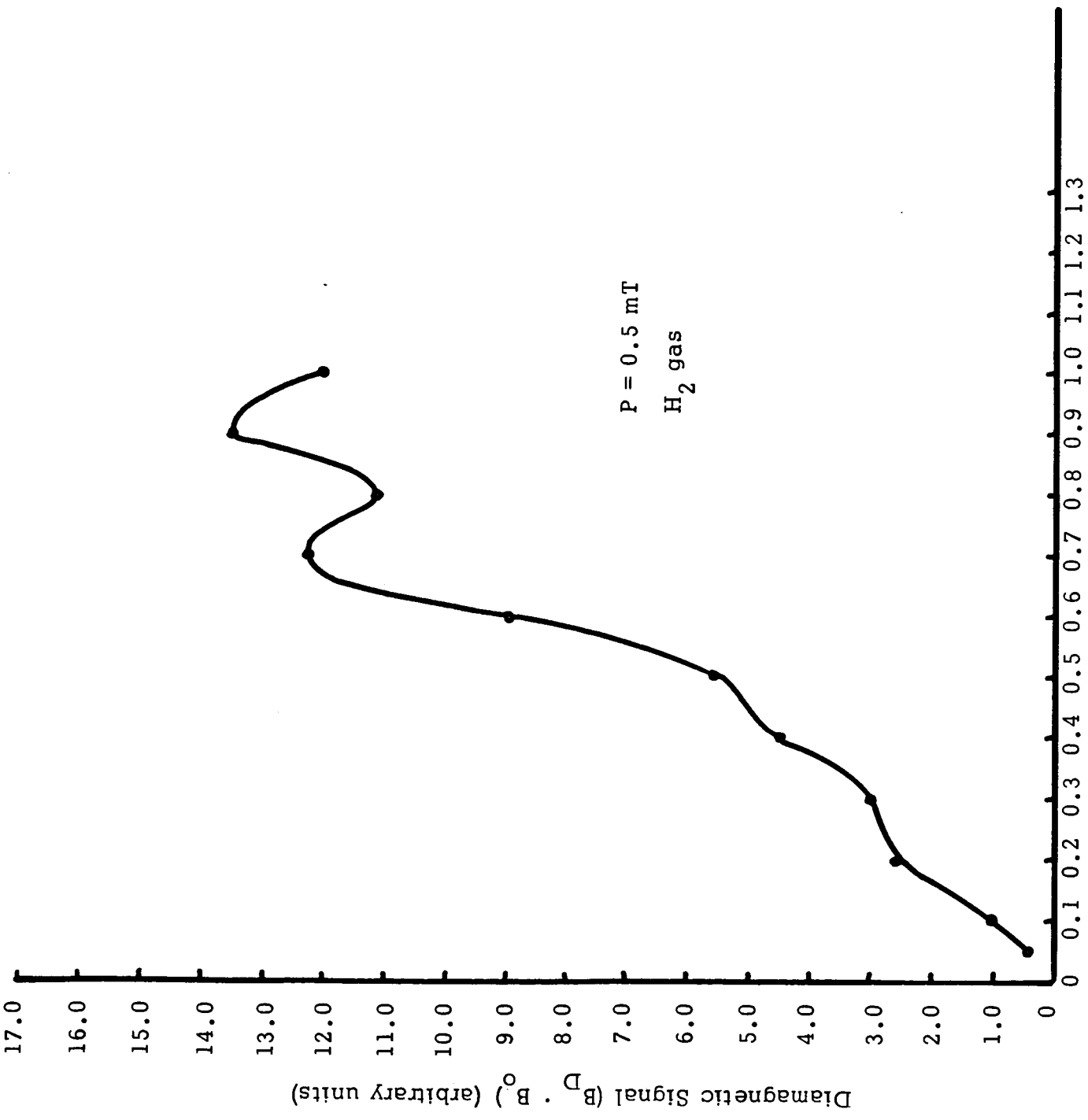

Fig. III-10. Diamagnetic Signal at 0.5 mT.

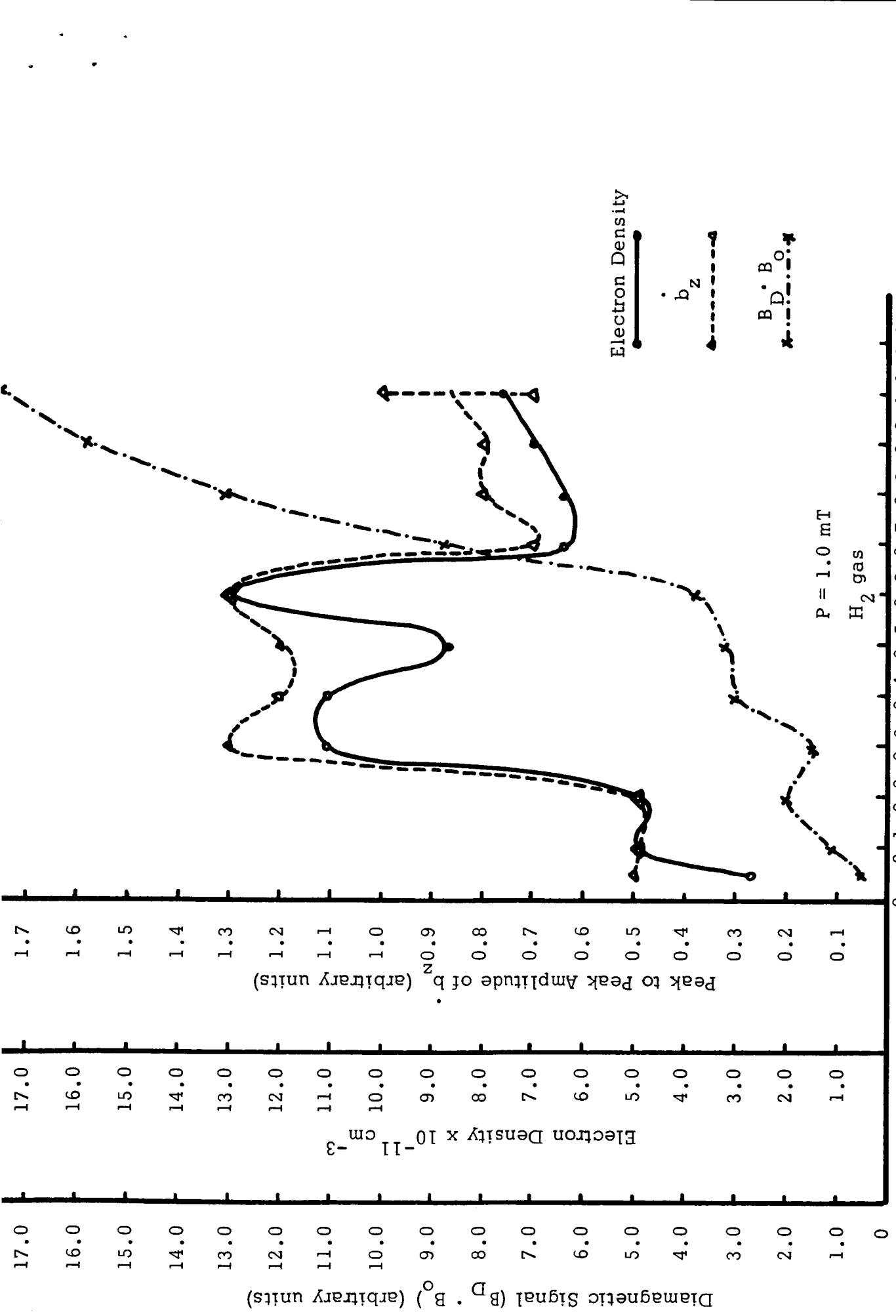

Fig. III-11. Comparison of Diamagnetic Signal to b_z (p-p) and Electron Density.

the wave phenomena was not exhibited. In this case, density, magnetic signal, and diamagnetic signal all decrease with decreasing magnetic field.

It is interesting to examine the $\dot{b}_z$ data by plotting curves of $\dot{b}_z$ versus neutral gas pressure for constant magnetic field B_o. Such a curve is shown in Fig. III-12 for B_o = 1.0 kG. The magnitude of magnetic signal gradually increases and peaks at about 0.8 mTorr, then gradually decreases. The bars in Fig. III-12 show the fluctuation of signal above 0.7 mTorr, which implies that although the amplitude of the propagating wave could be quite large, the wave tended to become cutoff more easily as pressure was increased. This behavior illustrates the fact, previously alluded to, that above about 1.0 mTorr there is a gradual "smearing out" of wave effects until all such effects are lost around 8-10 mTorr.

The peak in $\dot{b}_z$ occurs in all the curves of $\dot{b}_z$ versus pressure. As B_o is made lower, this peak gradually shifts slightly lower in pressure until it occurs at about 0.6 mTorr at 100G. At 300G, a double peak appears and a very strong cut-off region of neutral pressure occurs centered at 0.8 mTorr. This appears due to the widening of the cut-off regions discussed in Part A. The cut-off region is then displaced by the widening central propagation band and falls lower in the magnetic field range as the lower propagation band gradually disappears so that above 0.8 mTorr wave propagation once again occurs at 300G. This same effect is not as evident at other values of magnetic field between 0.1 and 1.0 kG.

The peaking of the electron density versus pressure curve is also quite pronounced, as seen in Fig. III-13, at B_o = 100G. It is notable that this peak occurs about 0.2 mTorr higher than the corresponding peak in $\dot{b}_z$. In general, however, the agreement between the two curves is quite close, as seen in Fig. III-14, at B_o = 500G, although there seems to be very little shift in the location of the peak density along the pressure axis. At 300G, the dip in $\dot{b}_z$ at 0.8 mTorr mentioned above parallels a corresponding minimum in electron density, which also exhibits a double peak behavior.

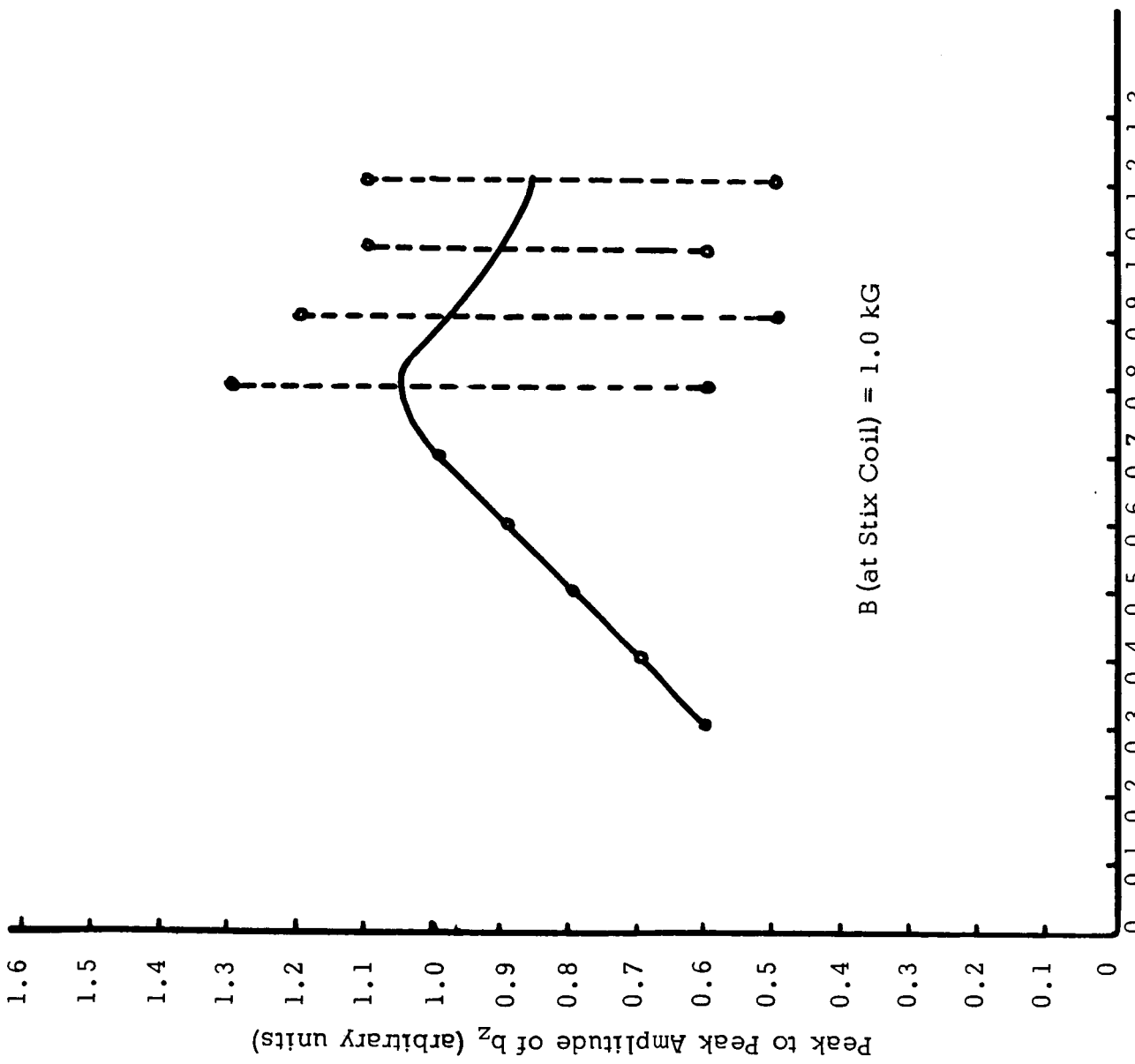

Fig. III-12. Amplitude of $\dot{b}_z$ (p-p) versus Pressure at 1.0 kG Showing Apparent Optimum Pressure at 0.8 mT.

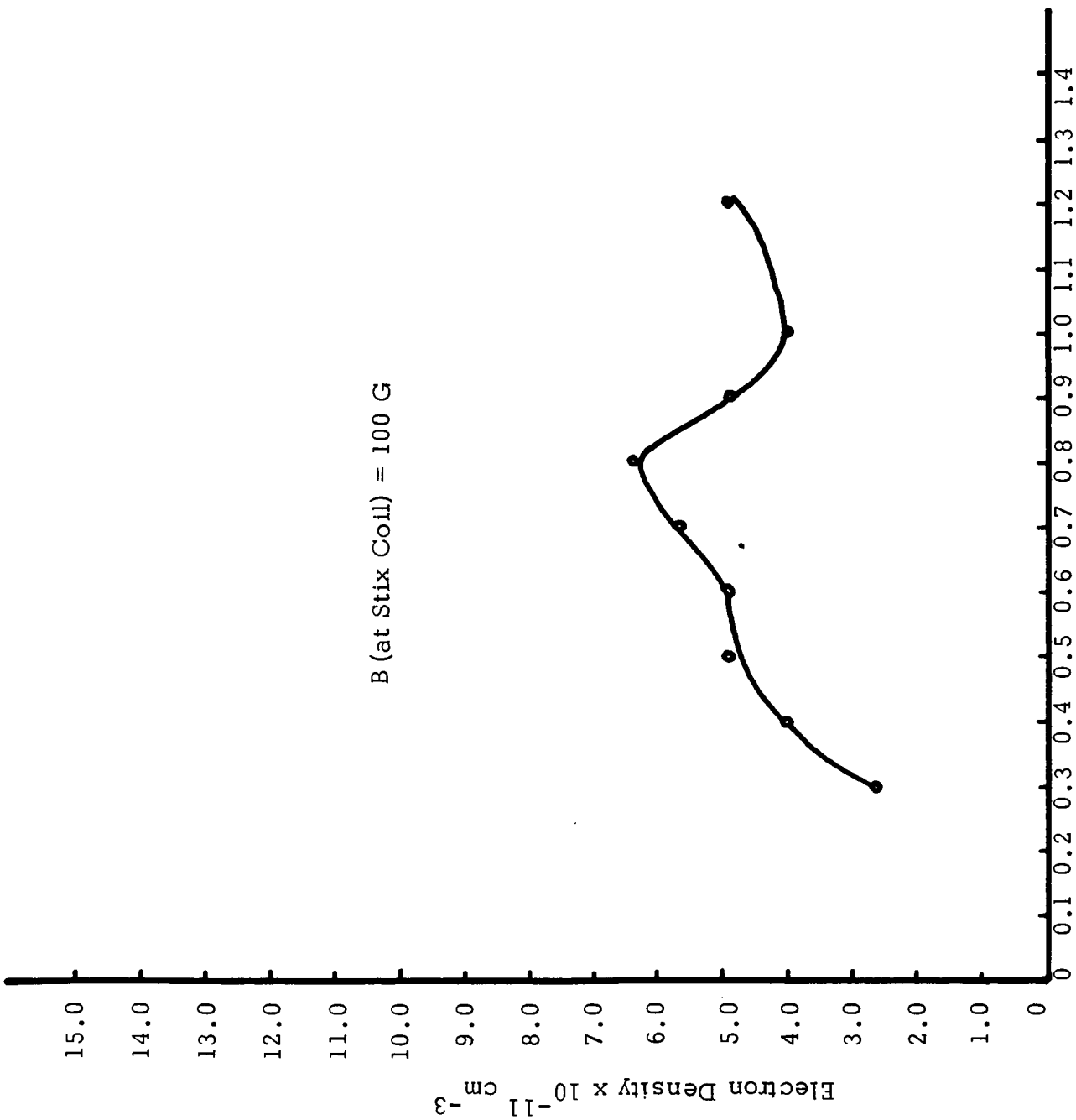

Fig. III- 13. Electron Density versus Pressure at 100 G, Showing Apparent Optimum Pressure at 0.8 mT, H_2gas.

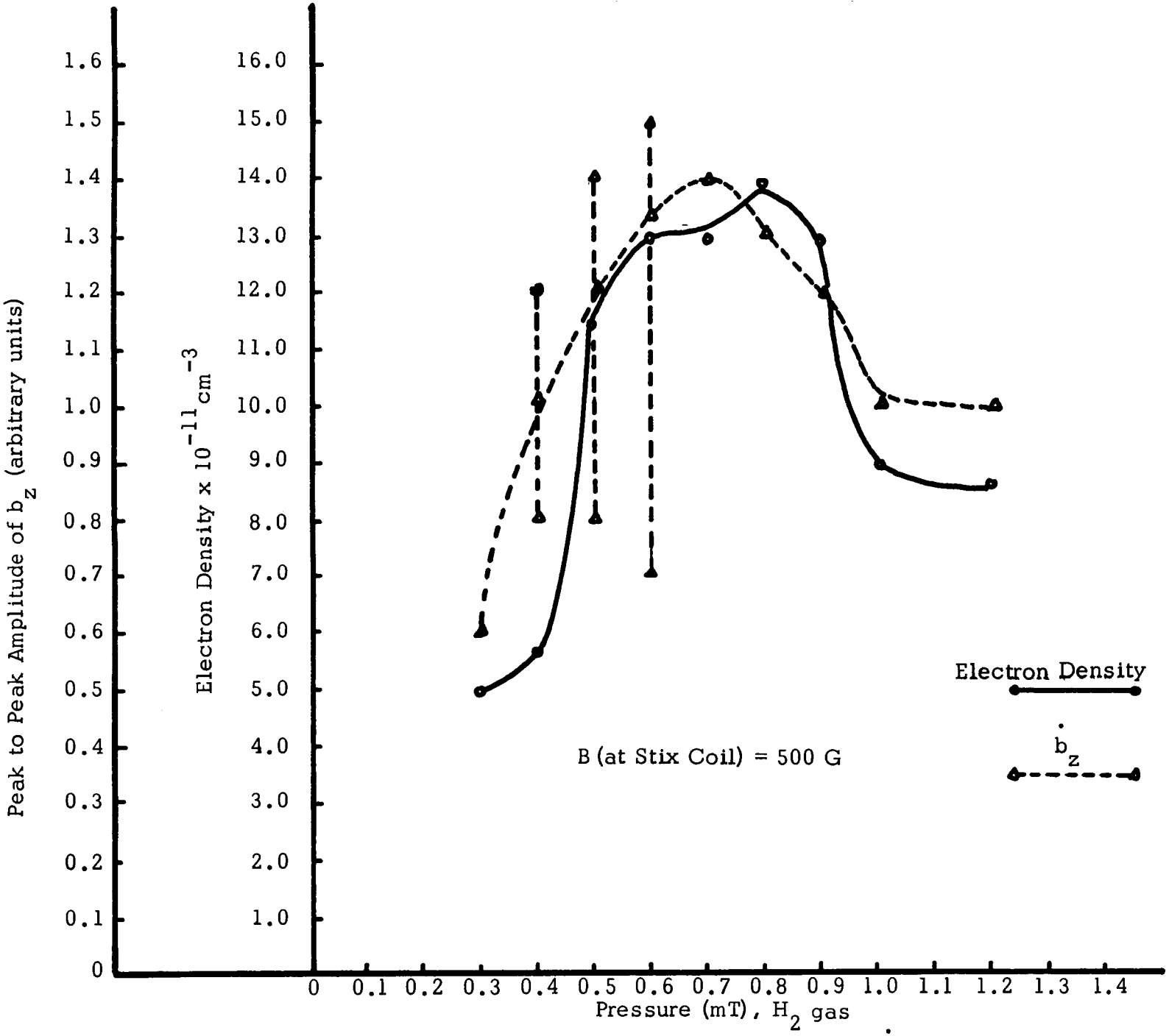

Fig. III-14. Comparison of Optimum Neutral Pressures for $\dot{b}_z$ and Electron Density at 500 G.

C. Low Magnetic Field Harmonic Frequency Phenomena

Work on nonlinear plasma phenomena[4] is extended here to the low magnetic field case. The method of detection of frequency spectra is identical to that reported previously.[4] The magnetic signal is terminated in a 50 ohm coaxial load, then passed through a 100:1 attenuator into a plug-in-amplifier unit in a Tektronix Model 555 oscilloscope. Previously, a Pentrix spectrum analyzer had been used as the plug-in unit, but a new Tektronix Model 1L20 spectrum analyzer has been obtained and was used in this series of experiments.

A typical photograph is shown in Fig. III-15a. The lower trace shows the magnetic signal being analyzed, while the upper trace gives the spectral content of the waveform. The far right vertical line of the graticle represents the lower end of the frequency scale, about 5 MHz, and the dispersion is 5 MHz/cm. The upper limit of the detector, in this case, is about 52 MHz, about half a centimeter from the left end of the scale. The spectral lines are broadened considerably because of the very rapid sweep required; the main rf pulse is only about 1 msec long. Although this is a compromise in that a slower sweep is desirable, the data is satisfactory since there is very little overlapping of the frequences which occur. Also, the reduction in amplitude due to the rapid sweep could be amply compensated for by the gain control on the analyzer.

A number of frequencies seem to be present in the magnetic signal over the entire range of the experiments. However, during wave attenuation, particularly at low fields, these harmonics become very substantial in amplitude. An example is shown in Fig. III-15b for the condition of 0.6 mTorr pressure at $B \simeq 50G$. The small spectral line on the far right represents the 5.8 MHz fundamental of the main rf transmitter; the second and subsequent "spikes" proceeding to the left are at harmonics of the 5.8 MHz fundamental, second through eighth. As noted in the last report,[4] a Tektronix Model 191 constant amplitude since wave generator was used in the identification of the various spectral lines.

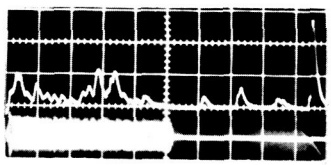

a. Spectrum (Upper Trace)

p = 0.7 mT

H_2 gas

B_o = 1000 G

Z = 50 cm

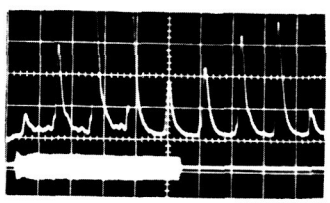

b. Spectrum (Upper Trace)

p = 0.6 mT

H_2 gas

B_o = 50 G

Z = 50 cm

Fig. III-15. (a.) Typical Spectrum from Plasma,
(b.) Spectrum During Wave Attenuation.

The occurrence of the harmonics lines seemed to be sensitive to magnetic field in a similar fashion to the magnitude of $\dot{b}_z$ and electron density. Fig. III-16 compares values of magnitudes of the 5.8 MHz fundamental and first harmonic (11.6 MHz) at 0.8 mTorr as a function of B_o. The curves seem nearly the inverse of one another in form, the maximum of the first corresponding to the minimum of the second.

The ratio of the magnitude of the 11.6 MHz signal to the 5.8 MHz signal may be taken as a measure of the amount of distortion present in the wave. The graph of this ratio at 0.8 mTorr is shown in Fig. III-17. It is interesting to note that this curve is an inverse to the plots of $\dot{b}_z$ and density at 0.8 mTorr; i.e., the minimum distortion seems to occur in the range of 400-600G where both $\dot{b}_z$ and density are at a maximum. Other harmonics of 5.8 MHz are also present, of course, but their behavior generally corresponds to that of the first harmonic. It therefore appears that maximum purity of spectrum occurs when wave propagation is strongest and electron density is high.

As a verification that the various frequency effects which have been noted are actually due to plasma-wave interactions, a current sensor was connected in the tuning circuit of the Stix coil. This sensor consisted of a small Rogowsky belt of about 100 turns wounds around a plexiglas form, connected to a BNC jack, and placed around the input strap to the Stix coil.

The current envlope and corresponding spectrum are shown at 0.8 mTorr, 100G in Fig. III-18a. In Fig. III-18b, $\dot{b}_z$ and its spectrum are shown (the narrow pulse is the 40 kW preionizer and was not in the time sequence being analyzed). The 5.8 MHz "spike" of the coil current spectrum is extremely large (it is hard to see in the figure, since the line is deflected off scale) with only very small harmonic lines, the double-peaked pulse on the far left being a transient in the spectrum analyzer and not a true spectral line. In contrast, there is a great deal of harmonic content in the $\dot{b}_z$ waveform. It is apparent that the harmonic phenomena occur in the plasma rather than in the transmitter or matching circuitry.

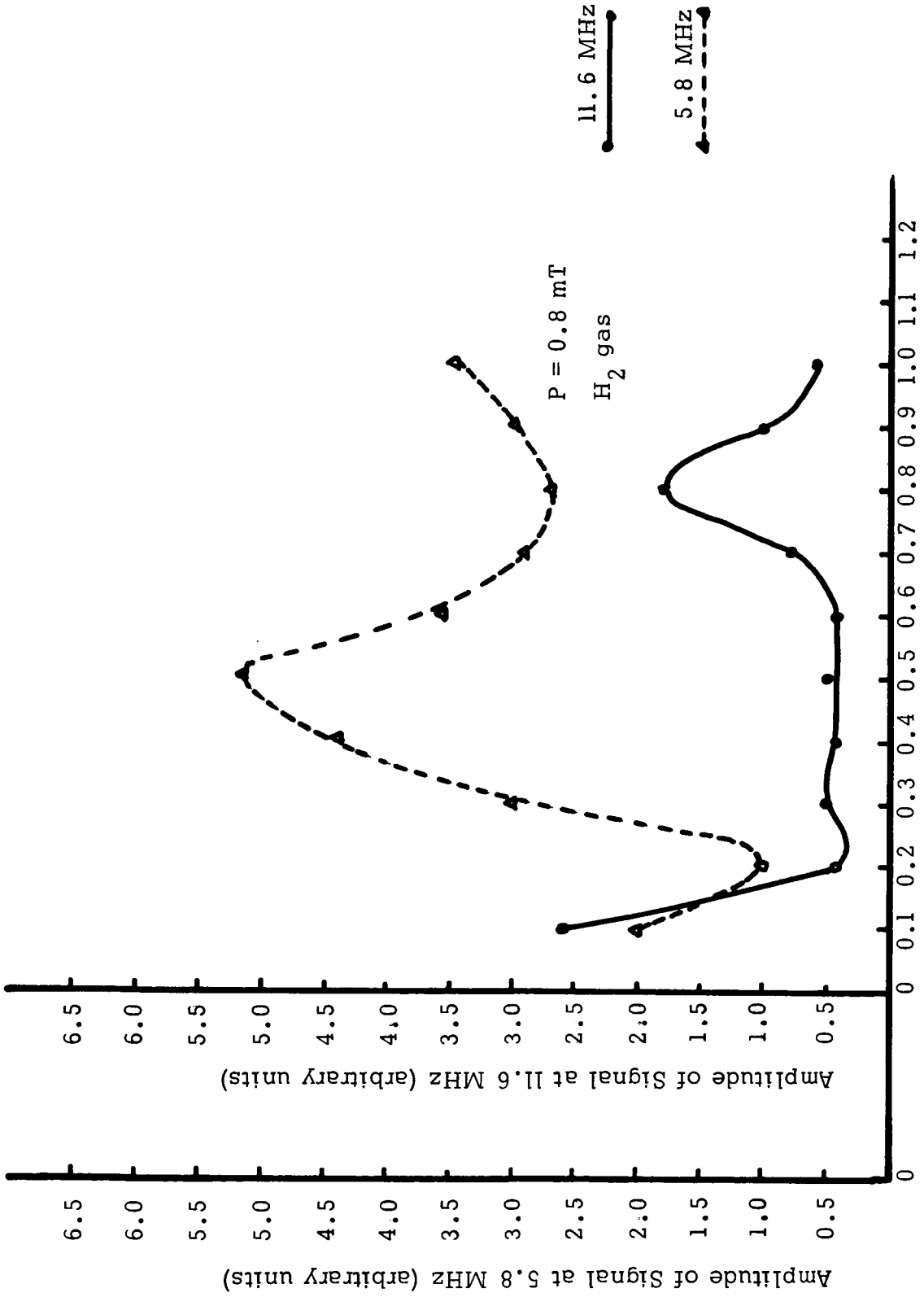

Fig. III-16. Amplitudes of 5.8 MHz and 11.6 MHz Signals from Plasma.

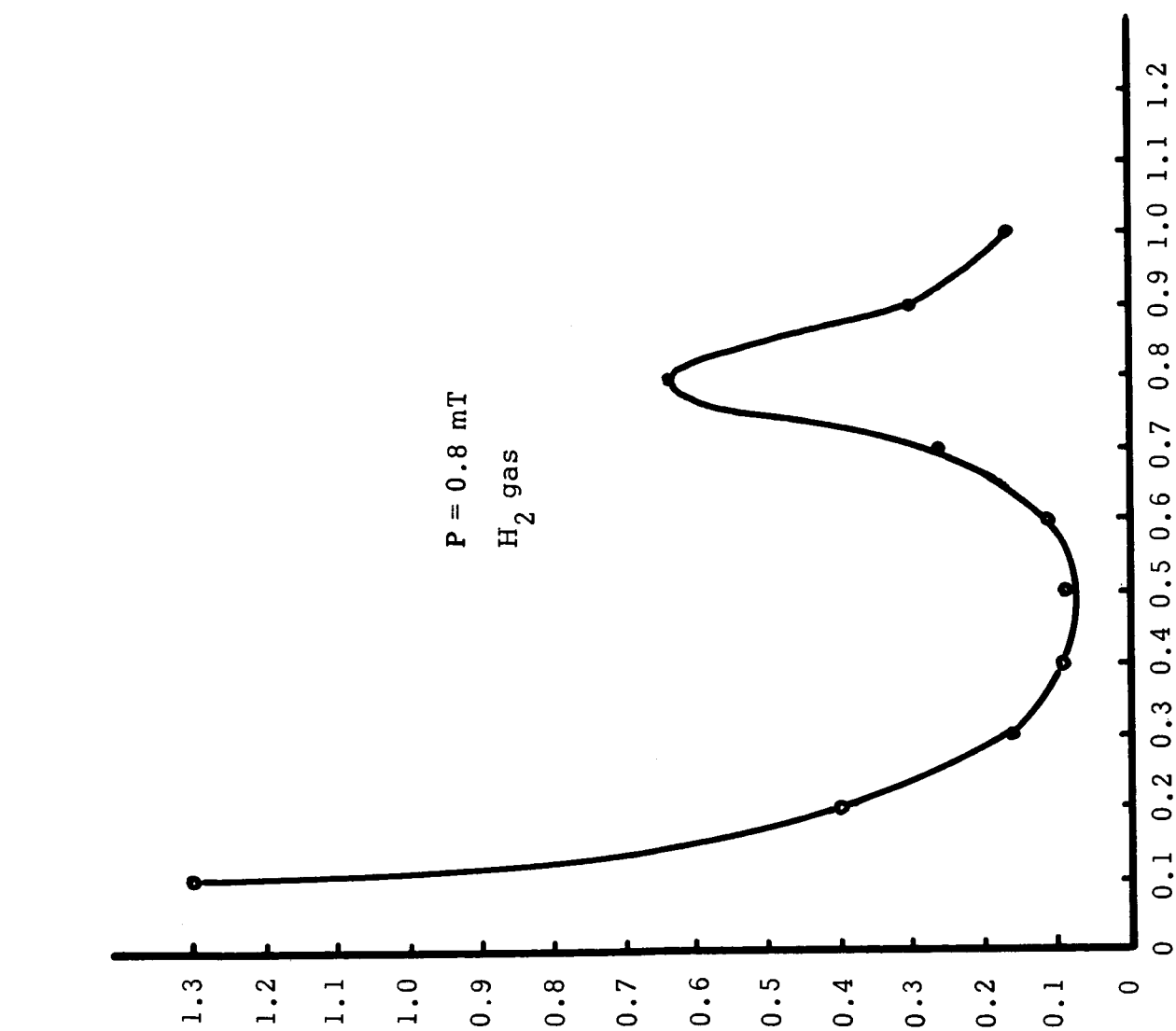

Fig. III-17. Ratio of Amplitude of 11.6 MHz Signal to Amplitude of 5.8 MHz Signal at 0.8 mT, H_2 gas.

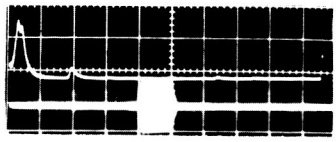

a. Coil Current Spectrum (Upper Trace)

p = 0.8 mT

H_2 gas

B_o = 100 G

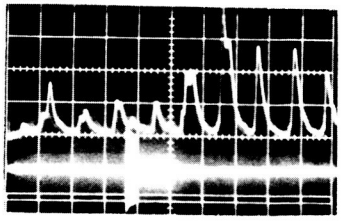

b. $\dot{b}_z$ Spectrum (Upper Trace)

p = 0.8 mT

H_2 gas

B_o = 100 G

Z = 50 cm

Fig. III-18. Comparison of Spectrum of $\dot{b}_z$ and Stix Coil Current During Wave Attenuation.

D. Discussion and Interpretation of Experimental Results

As mentioned in the introduction to Section III, the wave phenomena previously observed below 1.0 kG have been referred to as the so-called "fast" or right-hand circularly polarized hydromagnetic wave. More careful investigation, as described in Parts A-C of this section, reveals a complex behavior of the plasma which may allow as many as three bands of propagation in the range of 0.1 - 1.0 kG at a number of neutral pressures from 0.3 to 1.2 mTorr in hydrogen gas.

By examining the cold plasma dispersion relation for a cylindrical hydrogen plasma bounded by a vacuum, one finds[7]

$$\frac{\omega}{\Omega_i} > \frac{5.45\,(10)^7}{r_o}\left(\frac{1}{n_e}\right)^{1/2} \qquad \text{(III-3)}$$

for propagation of the "fast" hydromagnetic wave, where ω is the frequency of oscillation, Ω_i is the ion cyclotron frequency, r_o is the radius of the plasma, and n_e the electron density. At $\omega = (2\pi)\,5.8\,(10)^6$ (driving frequency in radians of the main rf transmitter), and taking the plasma radius to be 3.0 cm, we may write equation (III-3) as,

$$n_e > 2.28\,(10)^7\,B_o^2 \qquad \text{(III-4)}$$

where B_o is the static magnetic confining field, expressed in Gauss. For $B_o = 500G$, n_e must be greater than 5.7×10^{12} particles per cubic centimeter, a density higher than any observed in the data taken at 500G. Thus, it would appear that only the very lowest propagation band (50 to 75 G) observed could be the "fast" wave.

It should be emphasized that the laboratory plasma under consideration does not always fall under the classification of "cold" plasma. Moreover, radial density gradients may be present such that the peak density in the central core of the plasma is considerably above $5.7 \times 10^{12}\,cm^{-3}$, in which case "fast" wave

propagation would be possible along the central high density column. Thus, the propagation of the "fast" wave is not ruled out, although it seems unlikely at the higher values of B_o (i.e., for $B_o \gtrsim$ 300G).

A number of sources[2,3] have discussed plasma heating by the "fast" wave. Rothman and Chung[2] report better than 70 eV increase in the $(T_{e\perp} + T_{i\perp})$ sum, although the theory is not clear on heating with the right-handed wave. In particular, the above reference includes diamagnetic probe data supporting the findings quoted. The diamagnetic probe and supporting equipment used in the experiment at this facility are identical to those used previously[5,7] to report plasma heating by the ion cyclotron wave. The data obtained was satisfactory, and the behavior of the signal was as expected near $B = B_c$. Since the identical equipment was employed to take the data reported in Part B of Sec. III, the data appears to be authentic and to indicate a cooling of the plasma at low magnetic fields, which would not be characteristic of the fast wave.

Since the findings in the three preceding paragraphs are in agreement, it is tentatively concluded that the wave phenomena observed are not predominantly the "fast" hydromagnetic wave. It is anticipated that use of the low-current dc power supply discussed in Part E will facilitate the verification of the above conclusion by providing accurate values of low magnetic fields.

A number of possibilities have still to be considered among waves which might propagate at low magnetic fields. Among these are electron and ion acoustic waves and electrostatic ion and electron cyclotron waves. It should be pointed out that although these waves are primarily electrostatic in nature, there are small magnetic fields associated with them which could be detected using magnetic probes such as the $\dot{b}_z$ probe used here.

The most probable choices to consider are the ion acoustic wave and electrostatic ion cyclotron wave. Although no study of these waves has been attempted here for the case of a cylindrical plasma, the cold plasma modes for the unbounded case are well known in the literature.[8] Examination of the dispersion relation for the electrostatic ion cyclotron wave reveals that for electron

temperatures of interest (e.g., ~10 eV), the mode propagates only for $B_o \gtrsim 3.8$ kG, high above the magnetic field region of interest.

The ion acoustic wave is found to propagate at some angle θ to the magnetic field lines, or parallel to B_o, but perpendicular to B_o only near the limit as $B_o \rightarrow 0$. However, at the driving frequency of the main transmitter, the wavelengths involved are considerably larger than the dimensions of the laboratory plasma so that any ion acoustic oscillation would be strongly influenced by the boundary conditions imposed on the plasma.

Until more data is taken and theoretical work completed, the exact identity of the low-field wave phenomena remains unknown. What has become clear is that such phenomena seems a great deal more complex and of considerable more variety than was previously thought.

Reference to Fig. III-14 in Part B reveals an optimum pressure such that electron density is maximized around 0.8 mTorr, at $B_o = 500$ G. Since the electron density gradually decreases above 0.8 mTorr (and this decrease was noted at all magnetic fields in the 0.9 - 1.2 mTorr range), the percent ionization decreases rapidly. Thus, it is seen that the total number of neutral particles will be three orders of magnitude or more greater than the electron density by 10 mTorr. It is a reasonable result that in this pressure region, where ion-neutral collisions would be expected to become important, the low-field wave phenomena gradually disappear. It might be noted that around 8-10 mTorr the same "washing out" of ion cyclotron wave effects also occurs.

Part C deals with the nonlinear frequency phenomena observed at low magnetic fields. The amplitudes of most of the harmonic frequencies seems to increase markedly during attenuation of wave effects and diminish during strong propagation. This would seem to indicate that attenuation of the propagating wave is due to damping, either collisional or collisionless, from plasma-wave interaction (i.e., that plasma and wave are interacting). Because of diamagnetic signal measurements, however, from which a net temperature decrease is indicated, it appears that damping phenomena are not responsible for the wave attenuation.

Apparently wave cut-off occurs when propagation is no longer allowed by the varying parameters (n, B_o) and the boundary conditions imposed on the plasma, and the wave evanesces. The harmonic frequencies which then occur must be attributed to interaction of evanescing fields with the decaying plasma.

E. Plans for the Next Report Period

In the lower portion of its output range the 300 kW dc power supply is difficult to adjust to within $\pm$ 50 Gauss. The present plans call for substituting a low-current (0-100 a) dc power supply which will facilitate more accurate and easily controllable measurements in the region of 0-1000 G. Some of the measurements discussed in Parts A, B, and C will be repeated, and the series of experiments will be extended to deuterium. The magnetic field range in the experiments will be raised to include the top of the third apparent propagation band.

It is anticipated that further modifications in the microwave equipment will eliminate the noise problem and the need for modulation of the klystron. Electron density, diamagnetic signal, and harmonic frequency data will be taken as described above.

Investigation of applicable theory to the low-field propagation will be undertaken, and study of pertinent nonlinear theory leading to a better understanding of the harmonic and frequency phenomena will be continued. Spectrum data will also be taken in the region of propagation and damping of the fundamental ion cyclotron wave.

References for Section III

1. M. Kristiansen, J. G. Melton, F. C. Harris, N. B. Dodge and A. A. Dougal, S.S.R. No. 6 on NASA Research Grant NsG-353, Plasma Dynamics Research Laboratory, The University of Texas, Austin, January 15, 1966.

2. M. A. Rothman and K. Chung, "Heating of Plasma by the Fast Hydromagnetic Wave," MATT-Q-23, pp. 32-37, April, 1966.

3. M. A. Rothman, "Coupling of Waves to a Cylindrical Plasma," Technical Memorandum TM-217, Plasma Physics Laboratory, Princeton University, September, 1965.

4. J. G. Melton, N. B. Dodge and A. A. Dougal, S.S.R. No. 8 on NASA Research Grant NsG-353, Plasma Dynamics Research Laboratory, The University of Texas, Austin, January 15, 1965.

5. M. Kristiansen, F. C. Harris, N. B. Dodge, J. G. Melton and A. A. Dougal, S.S.R. No. 5 on NASA Research Grant NsG-353, Plasma Dynamics Research Laboratory, The University of Texas, Austin, July 15, 1965.

6. M. Kristiansen and A. A. Dougal, S.S.R. No. 7 on NASA Research Grant NsG-353, Plasma Dynamics Research Laboratory, The University of Texas, Austin, July 15, 1966.

7. W. M. Hooke and M. A. Rothman, "A Survey of Experiments on Ion Cyclotron Resonance in Plasmas," Nuclear Fusion, 4, pp. 33-47, 1964.

8. T. H. Stix, Theory of Plasma Waves, (McGraw-Hill Book Company, Inc., New York, 1962).